NASA

Technical Memorandum 86123

Geodynamics Branch Research Report - 1983

Edited by W. D. Kahn and S. C. Cohen

JUNE 1984

National Aeronautics and Space Administration

Goddard Space Flight Center
Greenbelt, Maryland 20771

USA 1976

LASER GEODYNAMIC SATELLITE (LAGEOS)

1	110
10	111
11	1000
100	1001
101	1010 .

Geodynamics Branch Research Report - 1983

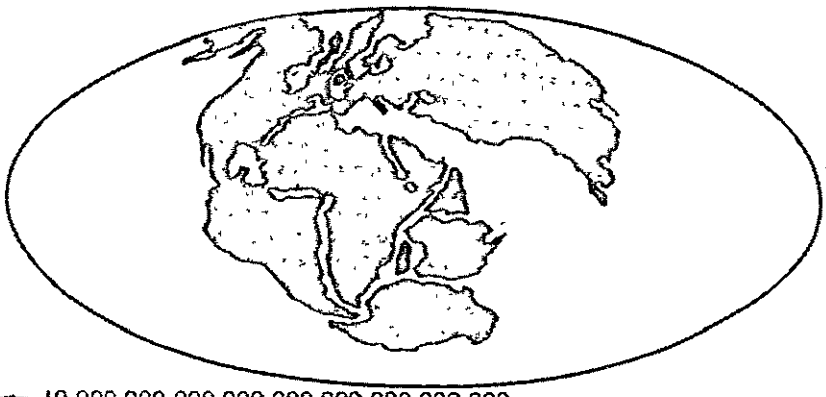

← 10 000 000 000 000 000 000 000 000 000 000

Edited by W. D. Kahn and S. C. Cohen

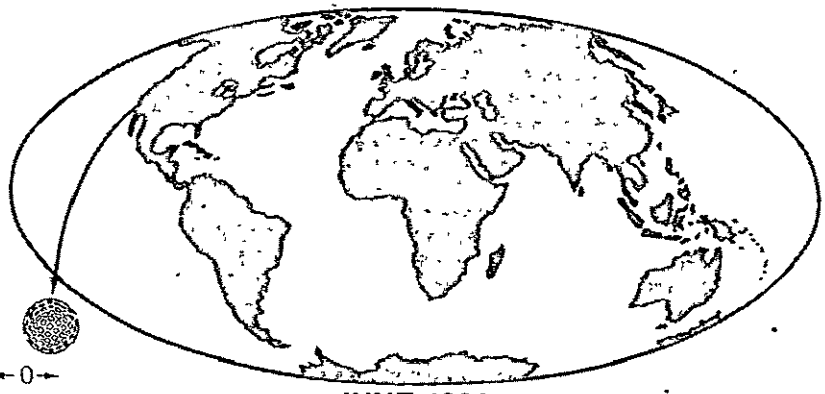

←0←

JUNE 1984

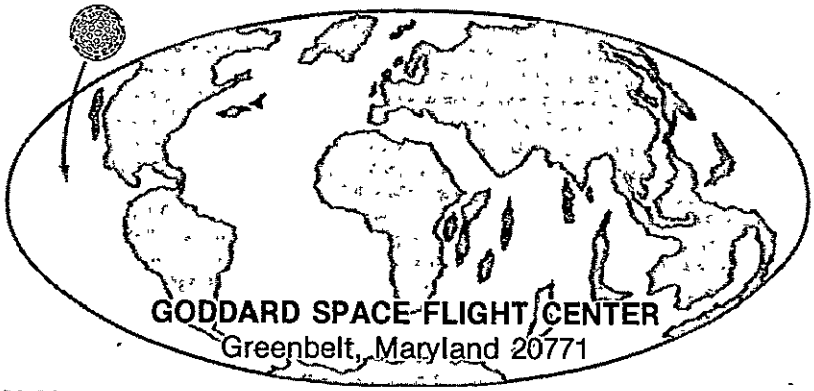

GODDARD SPACE FLIGHT CENTER

Greenbelt, Maryland 20771

100 000 000 000 000 000 000 000 →

GEODYNAMICS BRANCH STAFF

CODE 921

David E. Smith, Branch Head
Ph.D., 1966, University of London, Satellite Geodesy
Beatrice S. Boccucci, Secretary
Mary A. Melissa Wood, Secretary

Benjamin F. Chao, Ph.D., 1981, University of California (San Diego), Earth Sciences
Demosthenes C. Christodoulidis, Ph.D., 1976, Ohio State University, Satellite Geodesy
Steven C. Cohen, Ph.D., 1973, University of Maryland, Physics
Theodore L. Felsentreger, M.A., 1961, University of Maryland, Mathematics
Werner D. Kahn, M.S., 1955, University of Illinois, Mathematics
Chester J. Koblinsky, Ph.D., 1979, Oregon State University, Physical Oceanography
Ronald Kolenkiewicz, M.S., 1965, Catholic University, Space Science and Applied Physics
Francis J. Lerch, M.S., 1950, University of Delaware, Mathematics
Han-Shou Liu, Ph.D., 1963, Cornell University, Physics
James G. Marsh, M.S., 1963, West Virginia University, Physics
David C. McAdoo, Ph.D., 1976, Cornell University, Geophysics
Patrick H. McClain, M.S., 1959, Howard University, Mathematics
Barbara H. Putney, B.S., 1960, Brooklyn College, Mathematics
David P. Rubincam, Ph.D., 1973, University of Maryland, Physics
Braulio V. Sanchez, Ph.D., 1975, University of Texas, Aerospace Engineering
Frederick G. Schamann, B.S., 1967, City College of New York, Mathematics
Jean E. Welker, M.A., 1980, University of Maryland, Physical Geography/ History
George H. Wyatt, B.S., 1962, North Carolina State College, Mathematics

Resident Research Associate

Richard S. Gross, Ph.D., 1982, University of Colorado, Geophysics

CONTENTS

CONTENTS (Continued)

INTRODUCTION

This report is the second annual summary of the research program of the Geodynamics Branch. The branch is located within the Laboratory for Earth Sciences of the Applications Directorate of the Goddard Space Flight Center. The research activities of the branch staff cover a broad spectrum of geoscience disciplines including space geodesy, geopotential field modeling, tectonophysics, and dynamic oceanography. The NASA programs which are supported by the work described in this document, include the Geodynamics and Ocean Programs, the Crustal Dynamics Project, the proposed Ocean Topography Experiment (TOPEX), and the Geopotential Research Mission (GRM). The reports highlight the investigations conducted by the Geodynamics Branch Staff during calendar year 1983. The individual papers are grouped into chapters on Crustal Movements, Global Earth Dynamics, Gravity Field Model Development, Sea Surface Topography, and Advanced Studies. Further information on the activities of the branch or the particular research efforts described here can be obtained through the branch office or from the individual staff members.

OMIT

CHAPTER 1

CRUSTAL MOVEMENTS

OVERVIEW

Studies of crustal movements are devoted to the interrelated goals of determining tectonic plate motions, understanding their driving forces and the nature of plate interactions, and predicting the occurrence of earthquakes. The analysis of global and regional scale crustal movements provide information on seafloor spreading and continental drift, the creation and destruction of crustal material, and the structure, rheology, and dynamics of the earth's interior. Crustal deformation in seismically active zones provides information on strain accumulation and release, the state of stress in the earth's crust, and the mechanisms responsible for earthquakes. The work of the Geodynamics Branch includes activities in both the Crustal Dynamic Project which involves space geodetic observations and in the Geodynamics Research Program which involves basic studies into the dynamic processes of the earth.

This section of the Geodynamics Branch Report includes papers on the Measurement of Crustal Movements, Modeling of Earthquake Related Crustal Deformations, Modeling of Sublithospheric Stress Fields, and the Development of Satellite Tracking Facilities for Space Geodetic Measurements. The six reports are summarized as follows: 1) The first report is devoted to discussing recent results obtained from the San Andreas Fault Experiment. This decade long experiment has utilized satellite laser ranging techniques to monitor the broad motion of the tectonic plates comprising the San Andreas Fault System. 2) The second report focuses on the modeling of crustal deformation subsequent to an earthquake. The analyses are based on the physics of stress redistribution with time and distance from the seismic event and yields information on the rheology and structure of the earth's interior. 3) The third report discusses the results of Satellite Laser Ranging System collocation experiments performed to assess the laser system's performance prior to field deployment of the laser or during periods when the laser system's performance is degraded. 4) The fourth report describes how two different measurement techniques, namely Very Long Baseline Interferometry, and Satellite Laser Ranging compare in the measurement of distances between several locations in the continental U.S. 5) In the fifth report, the sublithospheric stress field in central Europe is derived from an analysis of the satellite-determined gravity field. The computed stress field is interpreted in terms of the regional seismicity, and geologic structure, and the phenomenon of gravity sliding of seismotectonic blocks. 6) The sixth report describes the result of error analyses undertaken to assess the quality of station coordinates, polar motion and earth rotation obtained from the analysis of laser ranging data from Lageos from March (1976) to the end of 1982.

Contributors to this chapter are: D.C. Christodoulidis, S.C. Cohen, R. Kolenkiewicz, H.S. Liu, J.W. Ryan, and D.E. Smith.

UPDATE:
SAN ANDREAS FAULT EXPERIMENT

Demosthenes C. Christodoulidis
David E. Smith

OBJECTIVE

A decade long experiment has utilized satellite laser ranging techniques to monitor the broad motion of the tectonic plates comprising the San Andreas Fault System.

BACKGROUND

Commencing in 1972, mobile laser stations have occupied sites on opposite sides and distances from the San Andreas Fault. This San Andreas Fault Experiment, (SAFE), has progressed through the upgrades made to laser system hardware and an improvement in the modeling capabilities of the spaceborne laser targets. Of special note is the launch of the LAGEOS spacecraft, NASA's only completely dedicated laser satellite in 1976. The results of plate motion projected into this 896 km measured line over the past eleven years are summarized and intercompared below.

RECENT ACCOMPLISHMENT

In satellite laser ranging the observed quantities are the nearly instantaneous ranges to a spacecraft and the times at which these distances are measured. If the evolution of the orbiting target and the rotational variations of the earth are accurately known, then the position of the observing station can be calculated in the geocentric reference frame used to describe the satellite motion.

With the launch of LAGEOS at high altitude, a laser target became available which was far less sensitive to the poorly known perturbing forces of short wavelength gravity and atmospheric drag. This is in marked contrast to the modeling problems found with BE-C, the spacecraft used for SAFE prior to launch of LAGEOS. With the development of a worldwide network of more advanced laser systems, the trajectory accuracies achievable for LAGEOS approach the quality of the laser tracking itself. Improved long wavelength gravity fields and highly accurate parameters to orient the earth's pole and rotation evolved from the analysis of the LAGEOS data. Thus, the requirement for specially "tailored" SAFE solutions as was done using BE-C data was no longer a necessity. The results obtained both from BE-C and Lageos data analyses are quite consistent and of a great deal of geophysical interest.

SIGNIFICANCE

A summary of the changes in the SAFE baseline lengths are shown in Figure 1. This figure is made somewhat complex due to the fact that the southern site for the experiment was changed from San Diego to Monument Peak, a distance of 50 km, during the course of the Crustal Dynamics Project. An adequate survey tie between San Diego and Monument Peak, comparable to the accuracy of the SLR measurements is lacking. Therefore, we have not attempted to present the length changes projected onto a single line, but rather, show changes in length over consecutive measures of the actual lines which were observed. Two independent sets of results from LAGEOS are compared to those from BE-C. One set of measurements (from 1976 to 1979) is coincident between the two satellites and directly compared.

Baseline lengths (referenced to an arbitrary set of origins) which were obtained from the laser tracking data are shown in Figure 1. A weighted fit of a straight line to each set of values was calculated to assess the rate of change in the length of the baselines. Since all these lines address the same broad tectonic motions, they can be combined to monitor an eleven year history of tectonic motion along the San Andreas Fault.

If the independent SLR rate measurements are assumed to be measures of the same constant tectonic rate, the weighted average rate for the last eleven years is -6.4 ± 1.0 cm/year with all measures agreeing to within their uncertainty. There is also a high level of agreement for the rates obtained using BE-C with those gotten from Lageos.

The satellite laser results can be compared to an independent estimate of tectonic motion. Minster and Jordan (1978) have made a global model of plate motion which reflects average plate motion (assuming rigid plates) over millions of years. Their model incorporates numerous data sources including earthquake slip vectors, transform fault directions and the spreading rate deduced from magnetic reversals at oceanic ridges. When using this model, the estimated rate of change for the San Diego to Quincy baseline is expected to be -5.6 cm/year. This value is within the formal error of our estimate of -6.4 ± 1.0 cm/year although it is hard to ascribe an uncertainty directly to the Minster and Jordan estimate.

FUTURE EMPHASIS

Satellite laser ranging has reached a new maturity with the launch of LAGEOS and the deployment of a globally distributed network of third generation trackers. The analysis of laser data has produced an eleven year history of inter-plate motion along the San Andreas Fault in California. The broad scale rate of motion between the

North American and Pacific Plates projected in the direction of Quincy to San Diego shows a baseline shortening of 6.4 ± 1.0 cm/years. This rate is in good agreement with the value predicted by the global tectonic model of Minster and Jordan (1978). Analysis techniques to improve the temporal resolution of the SLR measures are under development with preliminary results indicating that our standard annual solutions can be reduced to monthly or shorter samples of this inter-plate motion.

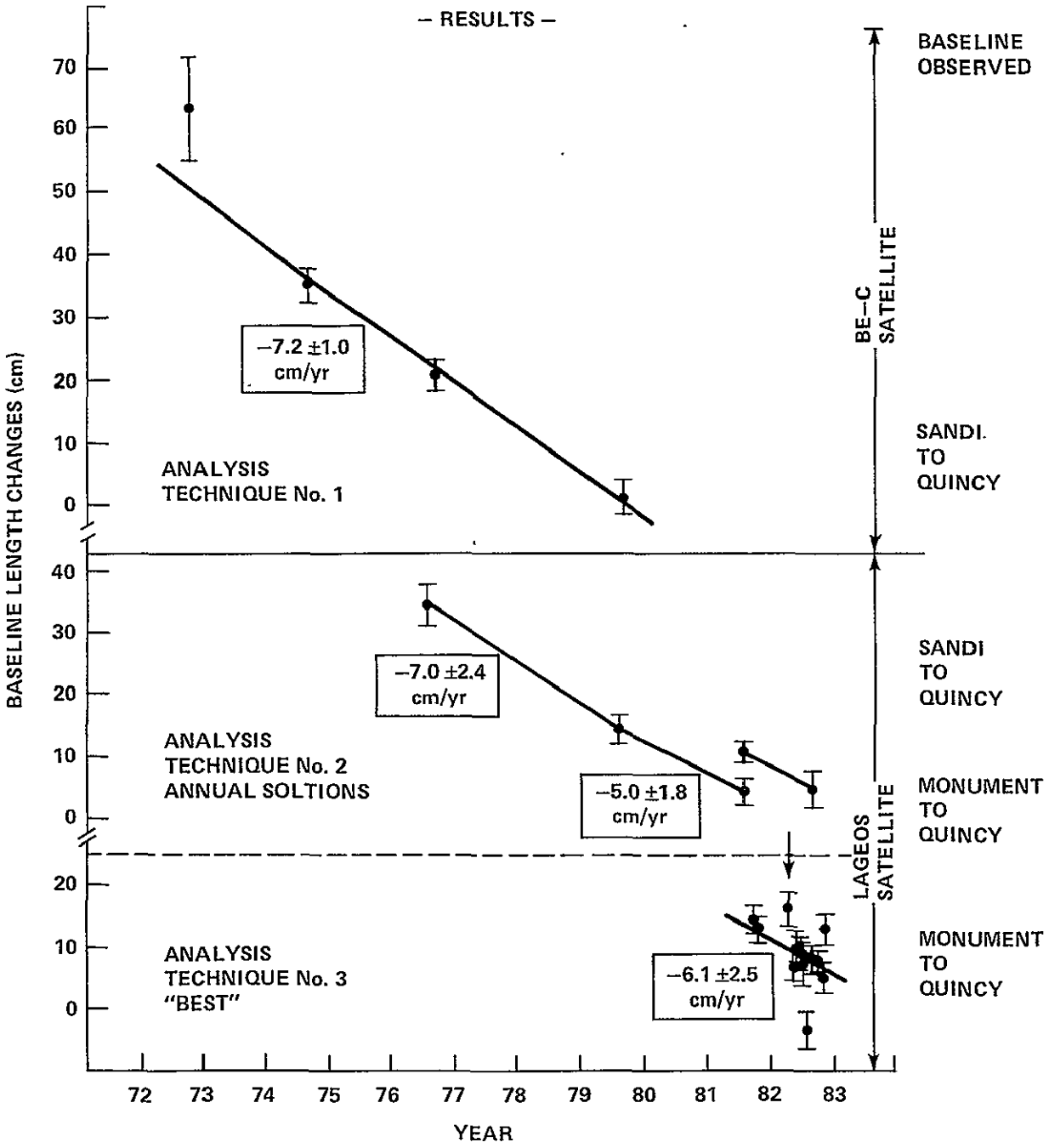

Figure 1. San Andreas Fault Experiment

CRUSTAL DEFORMATION AND EARTHQUAKES

Steven C. Cohen

OBJECTIVE

The purpose of this work is to develop an understanding of how the earth's surface deforms during the cycle of stress accumulation and release along major faults.

BACKGROUND

The spatial and temporal patterns of crustal deformation that accompany various phases of the earthquake cycle depend on the dynamical and structural properties of the stressed material in fault zones. The presence of viscoelastic material below the seismogenic zone in either the asthenosphere or in an intractrustal low viscosity zone has a pronounced effect on surface movement. The occurrence of an earthquake transfers stress from near surface elastic brittle material to deeper semi-fluid material. Viscoelastic flow of subsurface material in response to the stressing produces surface deformation due to the mechanical coupling between layers. The specific pattern that develops depends on the fault zone geometry, the thickness of the lithosphere and asthenosphere, and the viscosity of the semi-fluid material. Several different viscoelastic models of the earthquake cycle have been proposed for strike-slip geometries. These models, shown in Figure 1, differ in whether the asthenosphere is taken to be thin or thick and whether there are lateral variations in the mechanical properties of subsurface rock. Not surprisingly, the predicted deformation patterns associated with these models have significant dissimilarities. However the model differences arise not only from differences in physics but also from mathematical treatments employed to reduce the governing differential equations to a tractable form. The introduction of mathematical approximations can be largely overcome by employing finite element techniques uniformly to all the models. Numerical simulation of the earthquake cycle using the finite element approach permits model resolution and thereby improves our understanding of the details of the crustal deformation process.

RECENT ACCOMPLISHMENTS

It has been demonstrated that the surface crustal deformation pattern is sensitive mostly to the rheology of the material that lies below the seismic slip plane in a volume whose radius is a few times the fault depth. If this material is viscoelastic, the surface deformation pattern resembles that of an elastic layer over a viscoelastic half-space. However when the thickness or breadth of the viscoelastic material is comparable in size to

the fault depth, then the surface deformation pattern is altered by the geometry. In this case, geodetic measurements are potentially useful for studying the subsurface structure. Model differences are most detectable at intermediate distances from the fault (10^1 - 10^2 km) where the broad-scale features of viscoelastic flow have their clearest resolution. These differences are most pronounced shortly after an earthquake when the viscoelastic mechanisms generate signals much larger than those due to elastic mechanisms acting alone.

In an investigation of the crustal deformation associated with a thin channel asthenosphere it has been found that displacements are reduced from those computed for a half-space asthenosphere (see Figure 2). This result demonstrates that a previous finding by other workers that displacements are enhanced when flow is confined to a thin channel is based on several invalid approximations. The major predictions of the finite-element model are that the near-field postseismic displacements and strain rates are less than those for a half-space asthenosphere and that the postseismic strain rates at intermediate distances are greater (in magnitude). However the finite width of the asthenosphere ceases to have a significant impact on the crustal deformation pattern when its magnitude exceeds about three lithosphere thicknesses.

FUTURE EMPHASIS

The theoretical modeling aspects of the current research are now complete. The main thrust of current and future work is to apply the models to observed crutal movements and to extended finite element techniques to other crustal deformation processes such as continental collisions, postglacial rebound, and plate bending.

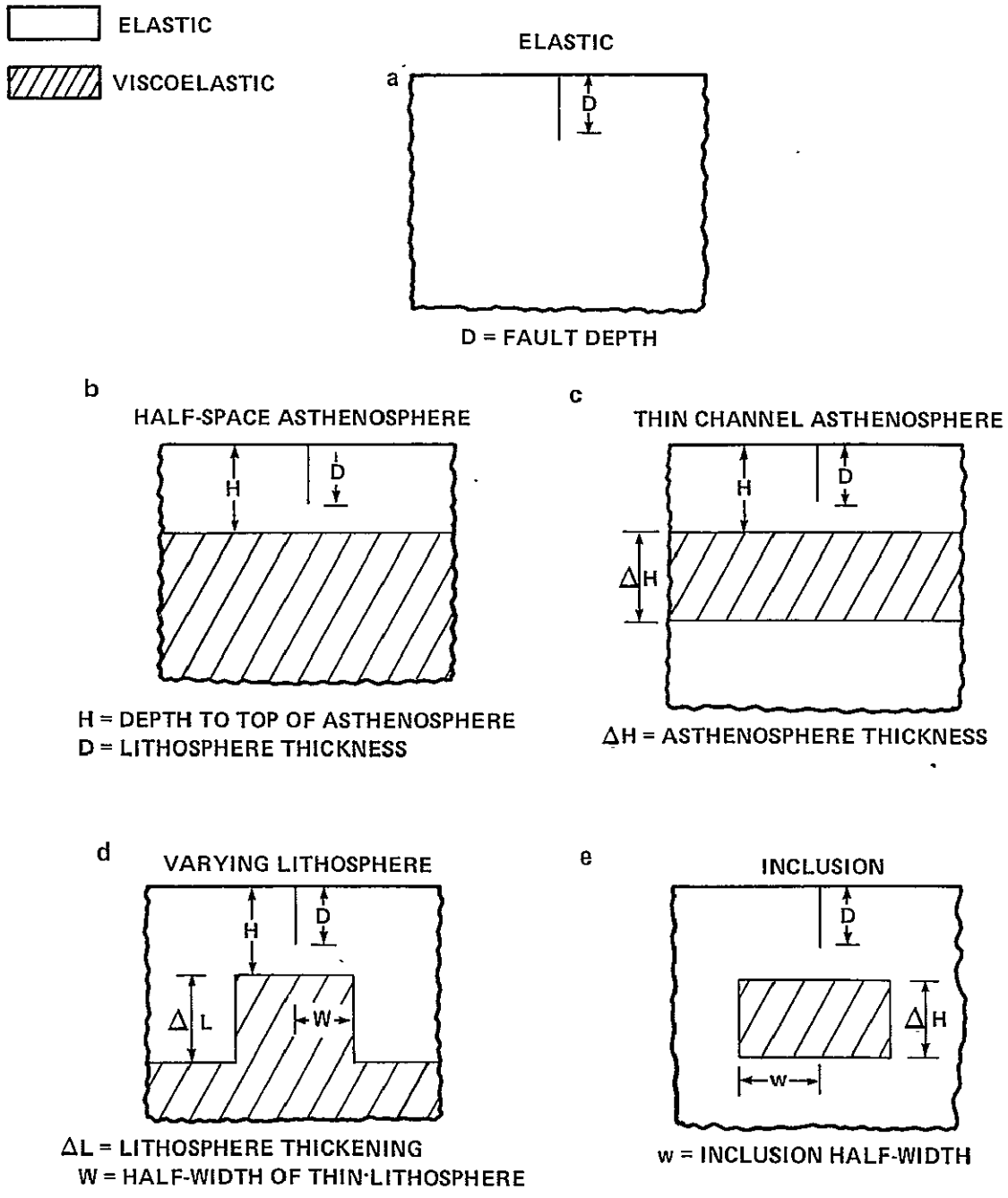

Figure 1. Models Used in Earthquake Cycle Simulations:
a. Elastic Half-space Model
b. Viscoelastic Half-space Asthenosphere Model
c. Viscoelastic Thin-channel Asthenosphere Model
d. Viscoelastic Varying Lithosphere Model
e. Viscoelastic Inclusion Model

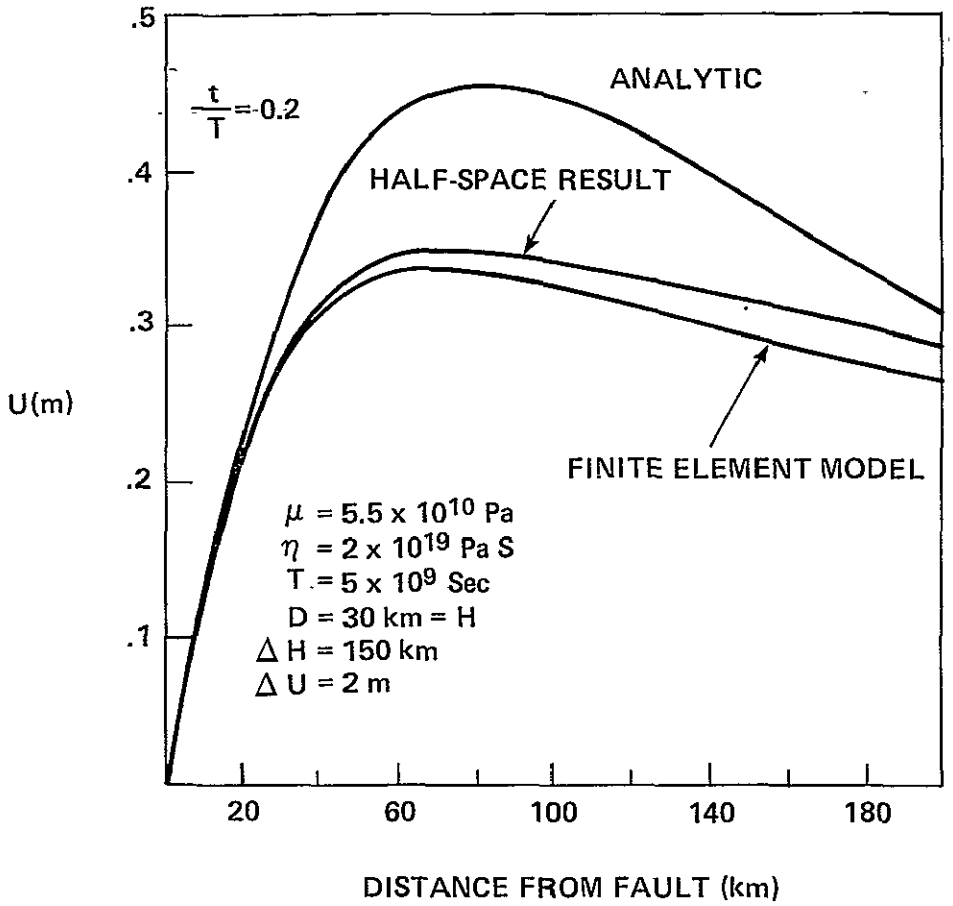

Figure 2. Comparison of Patterns of Displacement Versus Distance from the Fault for Thin Channel Analytic Model and Finite Element Model.

D3

RESULTS OF LASER RANGING COLLOCATIONS DURING 1983

Ronald Kolenkiewicz

OBJECTIVE

The objective of laser ranging collocations is to compare the ability of two satellite laser ranging systems, located in the vicinity of one another, to measure the distance to an artificial earth satellite in orbit over the sites. The similar measurement of this distance is essential before a new or modified laser system is deployed to worldwide locations in order to gather the data necessary to meet the scientific goals of the Crustal Dynamics Project.

BACKGROUND

For the direct study of crustal movements, position accuracies of a few centimeters are required over distances of hundreds or thousands of kilometers. Classical methods are inherently inadequate for this purpose. The space approach is to use an extraterrestrial reference system for determining the position of points on the Earth's surface.

One of the techniques applied by the Crustal Dynamics Project to do this uses laser ranging to satellites (i.e., measuring the time of flight of very short laser pulses to a retroreflector above the Earth's surface). This requires a high-altitude satellite whose orbital position can be determined to appropriate accuracy. The Laser Geodynamic Satellite (Lageos) is an example of a retroreflector equipped satellite in orbit, which is high enough to be free from serious perturbations caused by effects that are difficult to model (i.e., the complex gravity field structure attributable to density inhomogeneities in the Earth and variations in atmospheric drag). By knowing the satellite ephemeris, the position of a laser ranging station can be determined in an earth center-of-mass coordinate system.

In order to be certain the laser systems are operating properly, they are periodically compared with each other. These comparisons or collocations are performed by locating the lasers side by side when they track the same satellite during the same time or pass. The data is then compared to make sure the lasers are giving essentially the same range results. Results of the three collocations performed during 1983 are given.

RECENT ACCOMPLISHMENTS AND SIGNIFICANCE

During 1983 three collocation experiments were conducted viz:

1. Mobile laser system 4 (MOBLAS 4) was compared with mobile laser system 7 (MOBLAS 7) at Greenbelt, MD in May and June. The purpose of this collocation was to check out the newly upgraded MOBLAS 4 before deployment to Monument Peak, CA.

2. Mobile laser system 8 (MOBLAS 8) was compared with transportable laser system (TLRS 1) at Quincy, CA in July and August. This was a routine test to see how both systems were performing.

3. MOBLAS 4 was compared with TLRS 1 at Monument Peak, CA in October and November. MOBLAS 4 had been struck by lightning and its performance was being evaluated before it resumed its tracking operations.

A figure showing the mean residual difference (in centimeters), per pass of the satellite, between the two tracking systems is shown for each of the collocations (Figures 1,2, and 3).

In all cases the satellite tracked was Lageos. For example the collocation between MOBLAS 7 and MOBLAS 4 at Greenbelt, MD consisted of tracking the Lageos satellite by both lasers on thirteen separate passes. During the first pass, May 25, 1983, the MOBLAS 7 laser obtained 1050 range data points and MOBLAS 4 got 1395 points. Using these data an orbit was determined. The mean of the residuals (observed minus computed) about this orbit for MOBLAS 7 was -1.46 cm and for MOBLAS 4 was 0.84 cm. The difference of these means (MOBLAS 7 minus MOBLAS 4) is -2.30. In other words, for this pass, MOBLAS 7 was measuring shorter than MOBLAS 4 by 2.30 centimeters. The mean of these differences for the entire thirteen pass collocation was -2.95 ± 4.30 cm.

At this stage of evolution of the laser systems a criterion for a successful collocation requires that the mean of the differences obtained during the entire collocation be less then 3 centimeters. MOBLAS 4 marginally passed collocation and was transported to Monument Peak to join the satellite laser tracking network.

Figure 2 presents the Quincy collocation which yielded an RMS mean residual difference for eighteen passes of Lageos of -1.88 ± 3.29 cm. MOBLAS 8 and TLRS 1 are essentially yielding the same values ranging to the satellite and are considered to have a successful collocation.

Figure 3 shows the Monument Peak collocation for ten passes of Lageos. The RMS mean difference for these passes is 4.06 $\pm$ 1.60 cm. This is not a successful collocation between these two systems since there is a rather large bias (MOBLAS 4 longer by 4 cm) in the tracking data. This bias could be due to a number of things. Among them: (1) Either laser could be malfunctioning; (2) a survey error to the calibration board or between the lasers could have been made. MOBLAS 4 continues to track at Monument Peak and TLRS 1 has been deployed to other locations. Although useful systems they are still suspect until further analysis of the data has been completed.

FUTURE EMPHASIS

An attempt will be made to get better agreement between collocated laser ranging systems. This will be done by engineering changes to upgrade the systems, tighter constraints on the local surveys, and a review of current calibration and operation procedures.

ACKNOWLEDGMENTS

This work has been accomplished with the help of Van Hesson, Dave Edge, Win Decker, Mike Heinick and Vaughn Nelson, of the Bendix Field Engineering Corporation; Mark Torrence and Peter Dunn of EG&G Washington Analytical Services Center, Inc. and Mary Abresch of RMS Technologies, Inc.

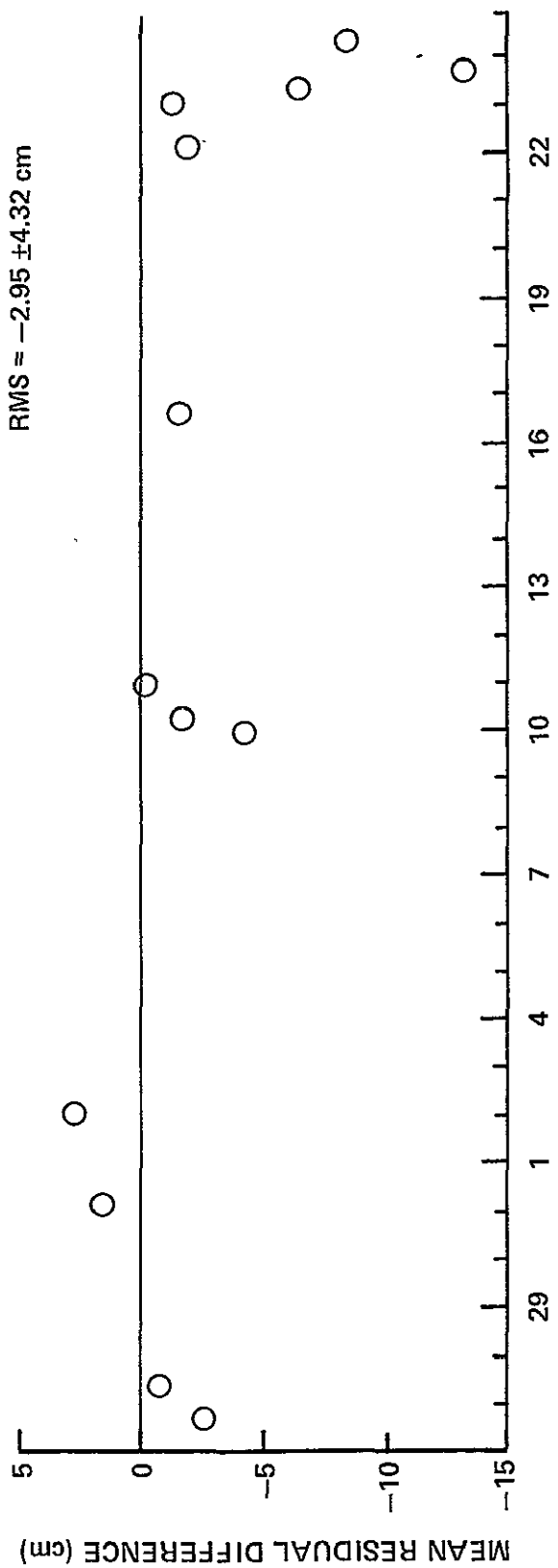

Figure 1. Greenbelt Collocation MOBLAS 7 Minus MOBLAS 4

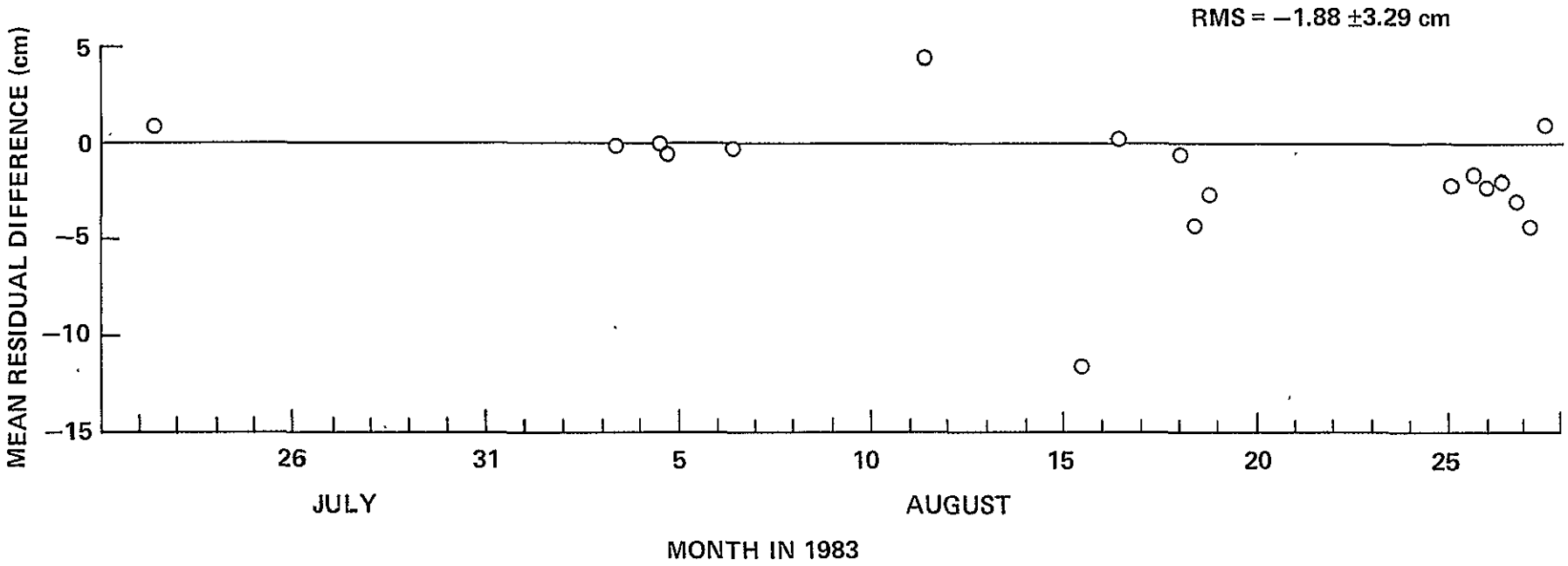

Figure 2. Quincy Collocation MOBLAS 8 Minus TLRS 1

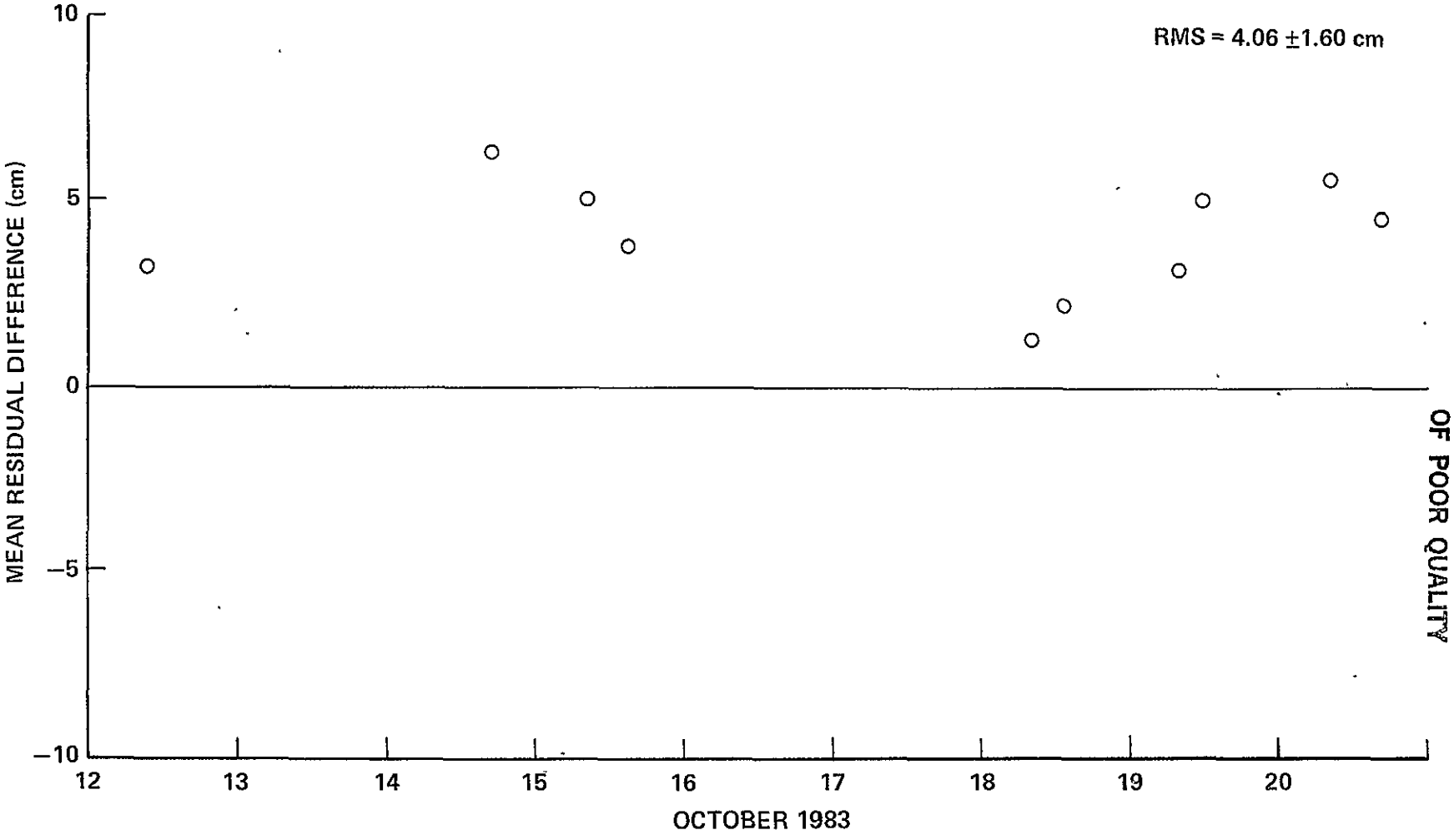

Figure 3. Monument Peak Collocation MOBLAS 4 Minus TLRS 1

D4

A COMPARISON BETWEEN LAGEOS LASER RANGING AND VLBI DETERMINED BASELINES

Ronald Kolenkiewicz
James W. Ryan

OBJECTIVE

The objective of this research is to determine how well two independent measurement techniques, Lageos satellite laser ranging (SLR), and very long baseline interferometry (VLBI) compare in the measurement of distances (or baselines) between several locations in the continental U.S.

BACKGROUND

The NASA Crustal Dynamics Project applies space methods and technology to advance the scientific understanding of earth dynamics. An important item in this understanding involves precise determination of position or rate of change of position in three dimensions and at places separated by hundreds-to-thousands of kilometers on the surface of the earth. The rates of change of position expected from geophysical and seismological considerations are approximately several centimeters per year, implying that over reasonable time scales, observational systems must be able to detect position changes of a few centimeters. These are the measurements that the Crustal Dynamics Project plans to collect, analyze, and interpret. Currently only two systems are capable of making these measurements, SLR and VLBI. In order to insure that the measurements are correct it is desirable to compare the results obtained by these systems.

Since October 1979 the SLR and VLBI elements of NASA's Crustal Dynamics Project have conducted coordinated experiments in which each technique independently measures the same baseline lengths. Sites occupied by the systems include: Westford, MA; Fort Davis, TX; Platteville, CO; and Owens Valley, Goldstone, Monument Peak, Quincy, and Pasadena, CA. Of the possible 28 baselines between these sites, 22 have been measured by both systems.

RECENT ACCOMPLISHMENTS AND RESULTS

Analysis of the data to produce the 22 sets of baselines for comparison has been completed. For SLR, Lageos laser data was analyzed in 92 30-day segments (ARCS) utilizing tracking data from a globally-distributed network and did not require simultaneous

tracking between observing stations. The parameters solved for in these arcs are the Lageos orbit, an along-track satellite acceleration, a solar radiation pressure coefficient, and polar motion and A1-UT1 every 5 days fixing the first A1-UT1 value in each arc. A value of GM and the latitude, longitude and height of each of the tracking sites (except the latitude and longitude of Arequipa, Peru and the latitude of Hawaii) were adjusted in common from all data. The force models employed included GEM-L2 gravity model with a recovered GM value of 398600.44 km^3/sec^2, Wahr's model for solid-earth tides and the Schwiderski Model was used to model the ocean tides.

The VLBI measurements were made during 24 days since August 1981. The observing sessions were used to produce 19 different solutions in which the VLBI antenna positions, source coordinates, clock parameters, and environmental parameters were adjusted. For the baselines that were determined more than once, a weighted average of the baseline was formed.

Local survey ties were made by National Geodetic Survey (NGS) at each tracking site to tie the VLBI and SLR systems together in a common reference system. This survey enables the baselines from one system to be calculated with respect to the other system. For these experiments the survey mark under the laser was the reference point. The local survey ties range in length from 16 meters to 8000 meters with conservative survey errors being no more than a few parts in 10^{-6}.

The results of this analysis is summarized in Table 1 where both the SLR and VLBI baseline lengths and their differences (SLR minus VLBI) are presented. A comparison of the 22 baselines shows a mean difference of 1.0 ± 1.1 cm with a scatter about zero of 5.2 cm. No apparent systematic scale difference betweeen the networks is evident.

Figure 1 is a map of the baselines and indicates their differences, SLR minus VLBI, in centimeters.

FUTURE EMPHASIS

Measurements between SLR and VLBI at additional sites in the continental U.S. will be made and compared. Of particular interest will be the future measurements made for the Monument Peak to Quincy, CA line. SLR has over a decade of history measuring across the San Andreas Fault, and the results show good agreement with existing tectonic plate theory (Minster-Jordan). VLBI has not measured this line frequently enough to draw similar conclusions at this time. Measurements for longer baselines, connecting North America and Europe, have been taken and will be compared.

ACKNOWLEDGMENTS

Mark Torrence and Steve Klosko of EG&G Washington Analytical Services Center, Inc. contributed to the SLR results.

TABLE I SLR AND VLBI BASELINES AND THEIR DIFFERENCES:
ORDERED BY LENGTH (CM)

FROM		TO	LENGTH	SLR	VLBI	SLR-VLBI
WESTFORD	-	PASADENA	405702200+	3	7	-4
	-	OWENS VALLEY	392972500+	83	77	6
	-	GOLDSTONE	390059500+	76	76	0
	-	FORT DAVIS	313863600+	10	16	-6
	-	PLATTEVILLE	275321900+	14	18	-4
FORT DAVIS	-	QUINCY	184183700+	85	79	6
	-	OWENS VALLEY	150127300+	80	76	4
	-	PASADENA	138369700+	73	63	10
	-	GOLDSTONE	129433300+	100	98	2
PLATTEVILLE	-	OWENS VALLEY	122172600+	61	67	-6
FORT DAVIS	-	MONUMENT PEAK	119828300+	84	76	8
	-	PLATTEVILLE	105568500+	89	85	4
QUINCY	-	MONUMENT PEAK	88360100+	80	79	1
	-	PASADENA	68574300+	28	32	-4
	-	GOLDSTONE	63970200+	98	94	4
OWENS VALLEY	-	MONUMENT PEAK	51088100+	1	8	-7
	-	QUINCY	38206700+	79	71	8
	-	PASADENA	33604200+	82	79	3
GOLDSTONE	-	MONUMENT PEAK	26365300+	71	76	-5
	-	OWENS VALLEY	25828900+	76	78	-2
PASADENA	-	MONUMENT PEAK	21828200+	80	80	0
	-	GOLDSTONE	17137400+	82	79	3
FOR 22 BASELINES			RMS ABOUT 0			5.2
			MEAN			1.0 ± 1.1

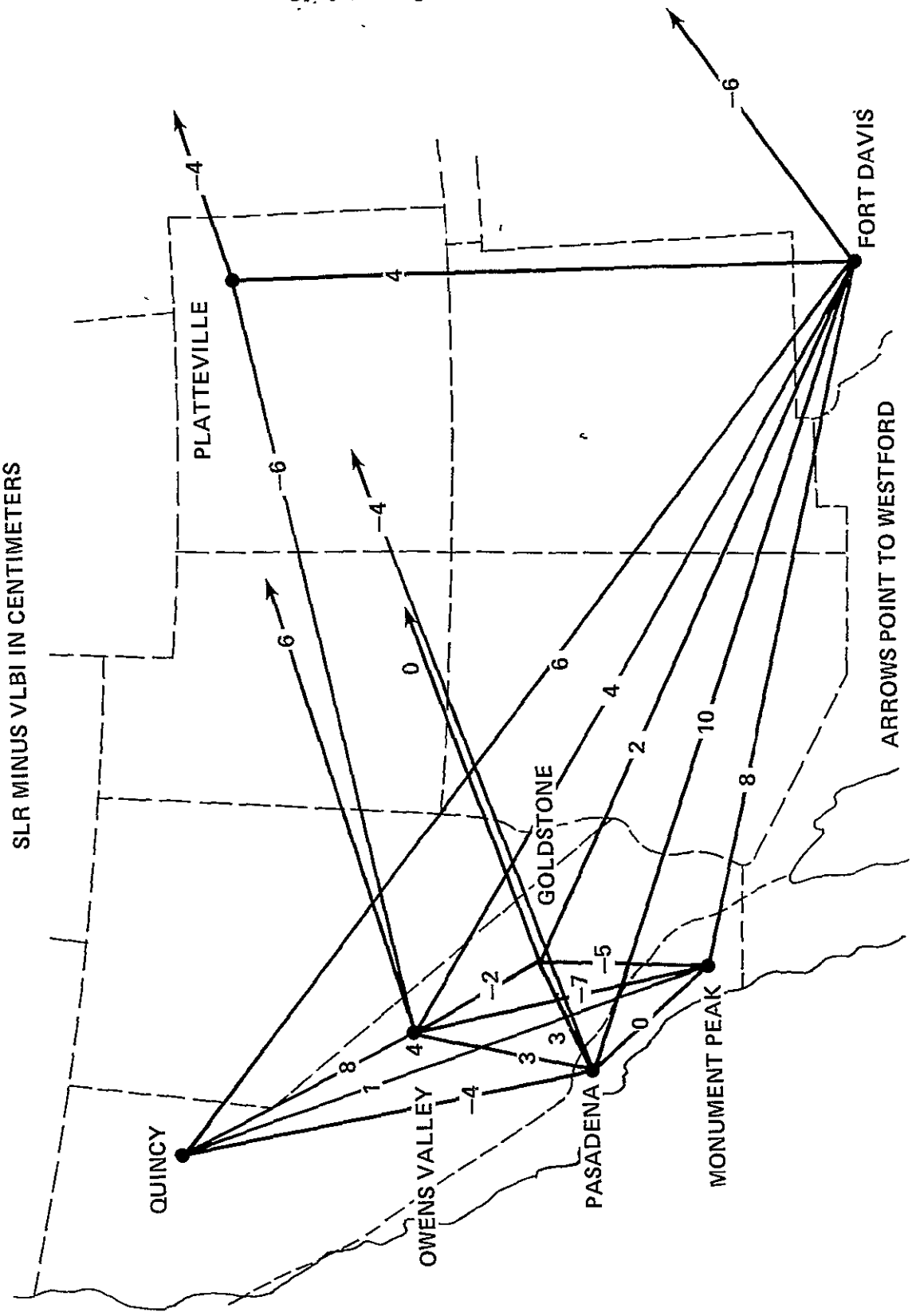

Figure 1. SLR and VLBI Intercomparison Lines

D5

GEODYNAMICS OF CRUSTAL DEFORMATION AND SEISMOTECTONIC BLOCK MOVEMENTS IN CENTRAL EUROPE

Han-Shou Liu

OBJECTIVE

Geological observations have revealed the style of neotectonic near-surface stresses and deformations in central Europe. Seismic activity, focal depths and fault-plane solutions of earthquakes indicate kinematic reactions within the crust. The objective of this study is to develop a crustal deformation which may account for the Rhine graben systems and the associated seismotectonic block movements in Europe.

BACKGROUND

The knowledge of seismic activity and tectonic structure in central Europe obtained by the European geoscientists is profound. It provides seismic, geological and geophysical facts to test whether the solutions of the focal mechanism for earthquakes, the distribution of orogenic activity, recent crustal block movements and upper mantle structure in this region can be integrated within a single Space Geodynamics Program.

The program for satellite measurement of the Earth's gravity offers a variety of models to interpret the interior of the Earth. Among the various interpretations, the subcrustal stress field serves as an intraplate parameter which corresponds to the lateral variations of gravity anomalies. In this study, a computer-aided tomography to gravity anomalies is used in determining the crustal stresses in central Europe. This study involves a search for tomographical interpretations of gravity data with respect to seismic stresses.

RECENT ACCOMPLISHMENTS

The subcrustal stresses can be inferred from satellite gravity data. Stresses at 6,000 grid points in Europe have been obtained by applying tomography to gravity field. Kinematics and dynamics have been integrated to show that the measured regional stresses in central Europe are derivable from the convection-generated traction on the boundary of the elastic spherical shell of the crust as inferred from satellite-derived gravity data. The stress pattern seems to suggest a seismogenic cause for the 1983 Liege earthquake which caused serious economic consequences in Central Europe.

SIGNIFICANCE

The stresses as shown in Figure 1 are comprised of several consistent stress patterns including the remarkable NW-SE compression under central Europe. By analyzing the satellite-derived stress fields in conjunction with tectonic and seismological observations in central Europe, we have obtained the following significant results:

1. Present-day stress field:
   The present-day stress field in central Europe can be obained from focal mechanism of earthquakes, orientation of geological joints and in situ stress measurements. The results of these seismic and geological observations are summarized in Figure 2. Figure 2 shows that the European crust is under NW-SE compression which is in full agreement with the satellite-derived stress field.

2. Orientations of the principal compressional and tensional stresses and the maximum shear stress in the crust of central Europe as inferred from satellite gravity data are shown in Figure 3 . These results have provided a dynamical basis for the deviatoric stress tensors and displacements in the epicentral areas of the historical earthquakes in central Europe.

3. According to the principles of crystal deformation, the stress components in the crustal block of central Europe can be modeled as shown in Figure 4. On the basis of this stress field--controlled crystal model of crustal deformation, the differing seismotectonic regimes of the Upper Rhine graben, the Lower Rhine graben and the Belgian and Swabian zones are easy to understand. Tensional crustal deformations are occurring under the influence of crustal stresses in a distinct manner only in the Lower Rhine graben, whereas in the other seismic zones, horizontal shear movements are more typical. Figure 4 shows that seismotectonic block movements in central Europe are clearly controlled by the stresses which are inferred from satellite-derived gravity data.

4. This study concludes that it is the stress field as inferred from satellite gravity data which determines such phenomena as rock stresses in mines, geological joints, earthquake mechanisms and seismotectonic block movements in central Europe. The crustal stress field in central Europe computed on the basis of satellite data gravity resembles closely the experimental pattern of single-crystal deformation. It has been shown that much of the intraplate deformation in central Europe can be explained by the dynamical processes that govern single crystals which are a billion times smaller in size than seismotectonic blocks.

FUTURE EMPHASIS

European seimsologists are largely tutored in certain branches of mathematics, and quite prepared for this unorthodox approach to seismic activity in Europe. When the European geoscientists could not understand the mystery of the Liege earthquake (November 8, 1983), this approach could probably be used as a last resort. It is emphasized that future analysis of stress concentration as inferred from satellite gravity data should provide a seismogenic model for the strain release pattern in central Europe.

REFERENCES

Ahorner, L., 1975. Present-Day Stress Field and Seismotectonic Block Movements Along Major Fault Zones in Central Europe, Tectonophysics, 29, 233-249.

Gagnepian-Beyneix, J., 1982. The Pyrenean Earthquake of February 29, 198: An Example of Complex Faulting, Tectonophysics, 85, 273-290.

Greiner, G. and Illies, J.H., 1977. Central Europe: Active or Residual Tectonic Stresses, Pure and Applied Geophysics, 115, 11-26.

Liu, H.S., 1983. A Dynamical Basis for Crustal Deformation and Seismotectonic Block Movements in Central Europe, Physics of the Earth and Planetary Interiors, 32, 146-159.

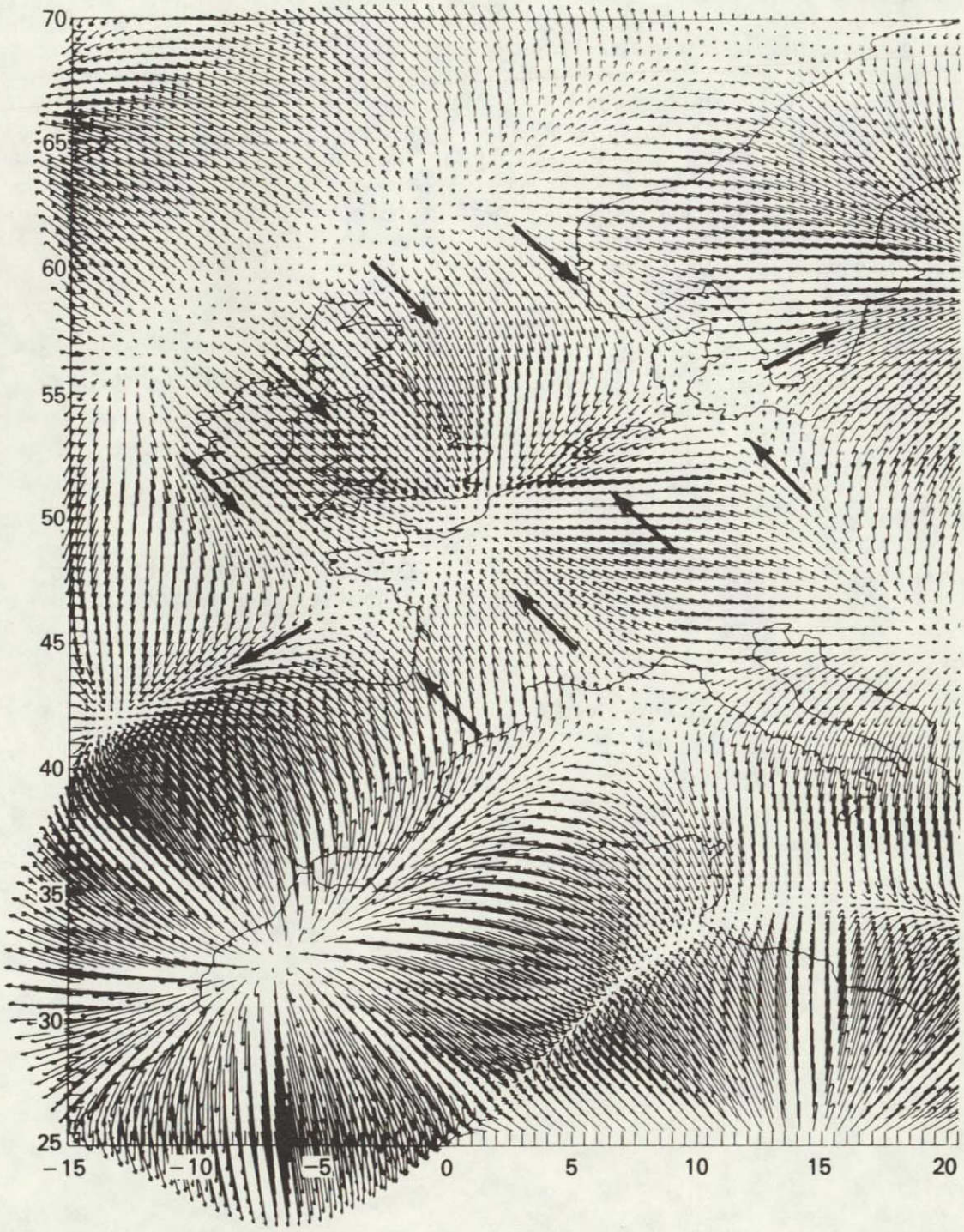

Figure 1. Subcrustal Stresses Under Europe as Inferred from Satellite Gravity Data.

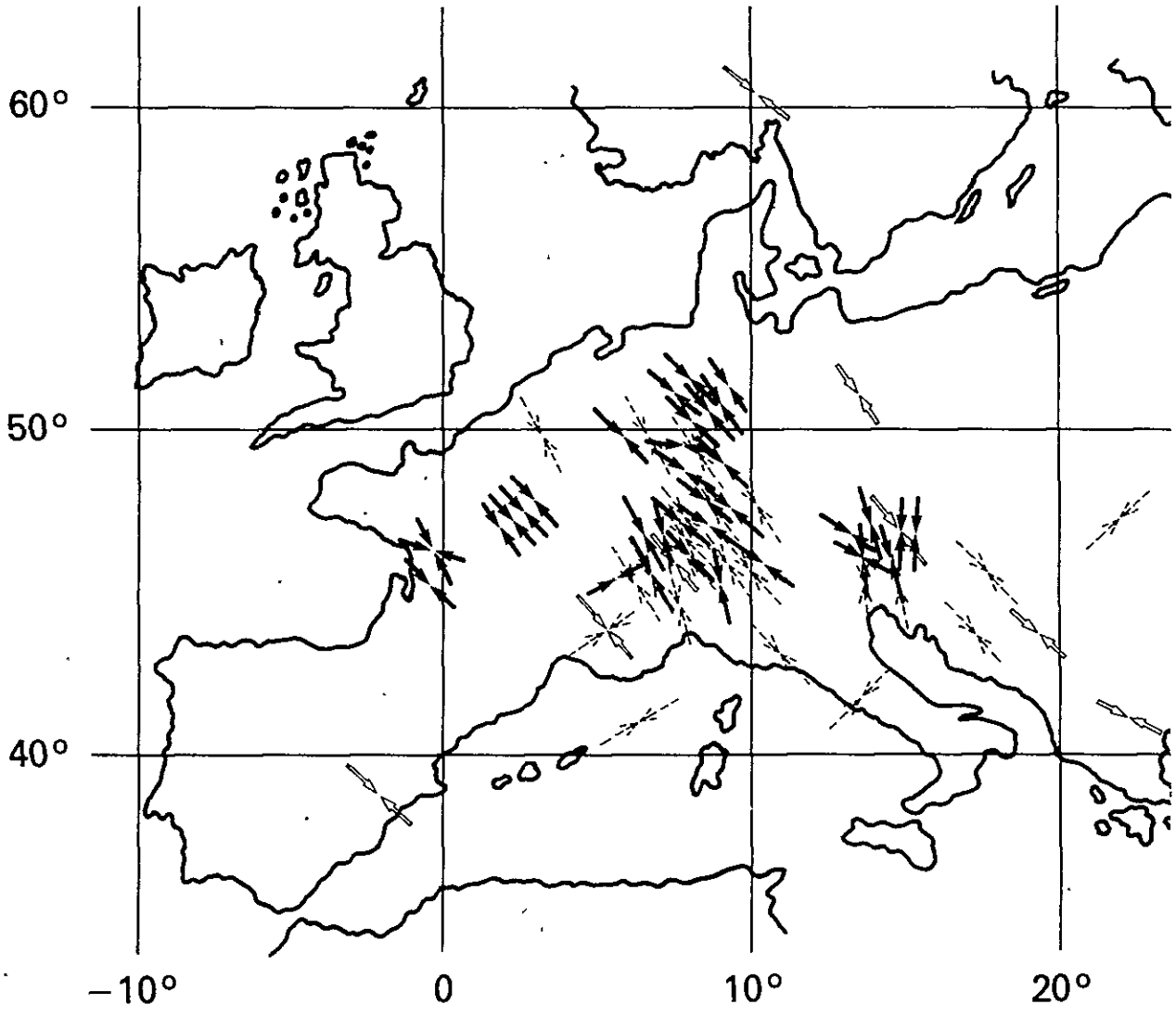

Figure 2. Present-day Stresses in Central Europe Deduced from Seismic and Geological Phenomena.

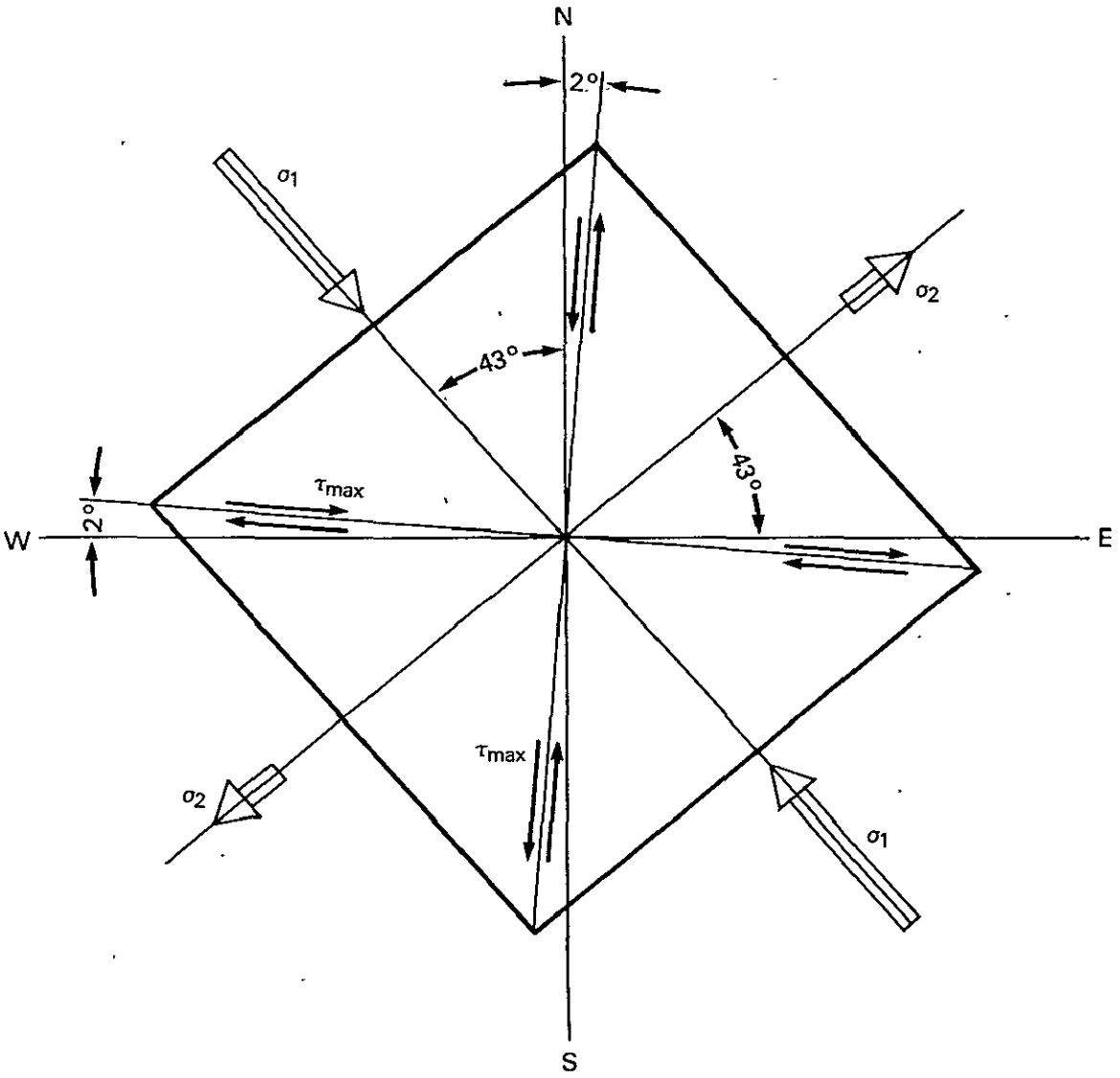

σ_1 PRINCIPAL COMPRESSIONAL STRESS
σ_2 PRINCIPAL TENSIONAL STRESS
τ_{max} MAXIMUM SHEAR STRESS

Figure 3. Orientations of the Principal Stresses in the Crust of Central Europe as Inferred from Satellite Gravity Data.

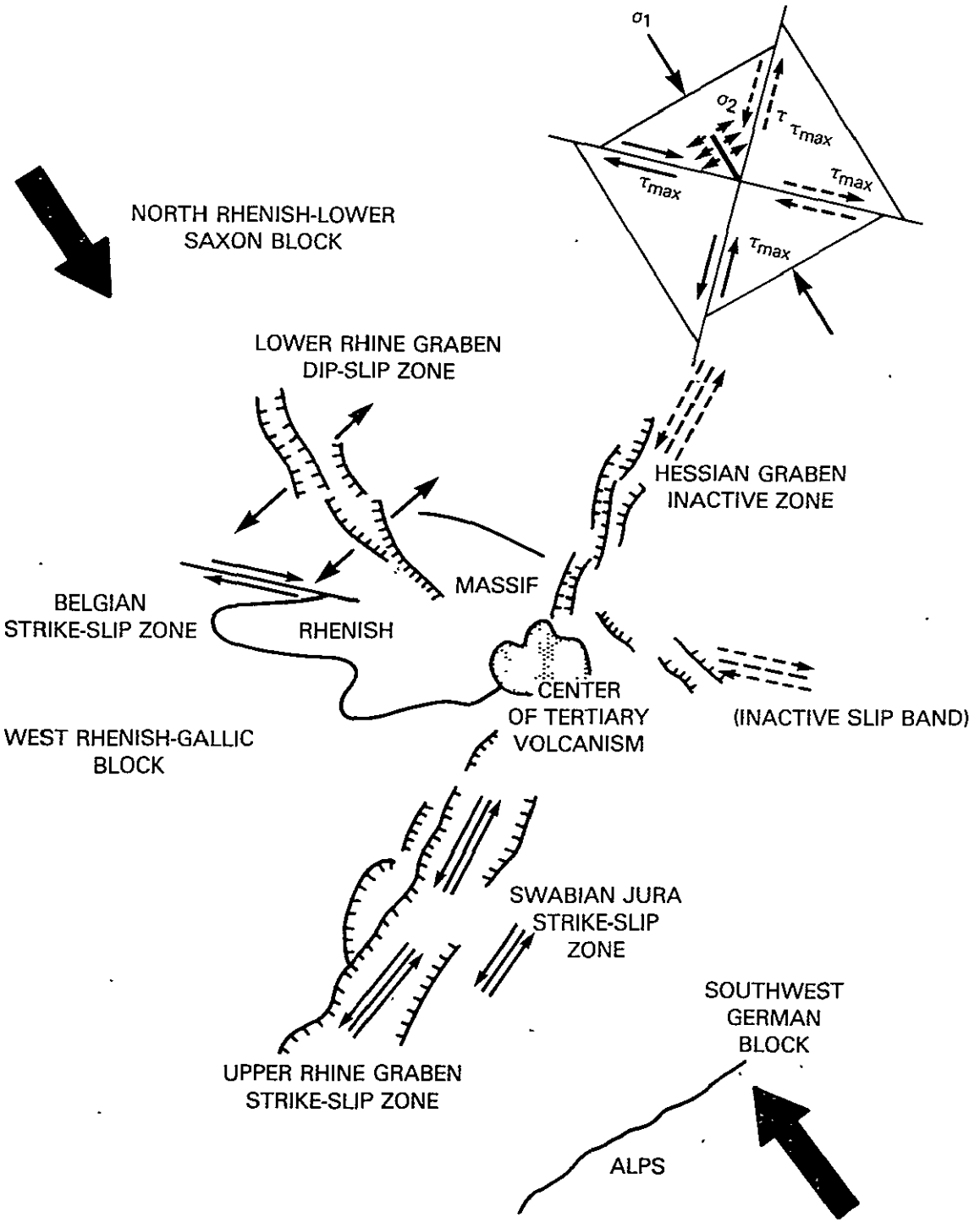

Figure 4. Seismotectonic Scheme of the Rhine Graben System with the Calculated Crustal Stress Components and Possible Horizontal Crustal Block Movements.

D6

N84 30461

SENSITIVITY OF SLR BASELINES TO ERRORS IN EARTH ORIENTATION

David E. Smith
Demos C. Christodoulidis

OBJECTIVE

To assess the sensitivity of inter-station distances derived from Satellite Laser Ranging (SLR) to errors in earth orientation.

BACKGROUND

The limiting factor in dynamical satellite geodesy for estimating station coordinates is clearly our degree of understanding of the evolution of the orbit and the precise positioning of the earth with respect to the orbit in time. In practice, the laser ranging data acquired on Lageos is of sufficient abundance and quality to permit the satisfactory simultaneous solution of polar motion, earth rotation and station parameters in a least squares adjustment procedure (to within an undeterminable absolute longitude constant) because each has a unique signal within the laser range data. While this procedure has essentially eliminated errors in earth orientation as a source of concern, an error propagation has been undertaken to fully assess the quality of the results should some externally-derived values of polar motion and UT1 parameters of unknown error be adopted as a reference within our multi-year solutions.

RECENT ACCOMPLISHMENTS

An analysis experiment has been performed within our multi-year (from the launch of Lageos in 1976 to the end of 1982) solution which imposed a known polar motion error on all of the orbital arcs used over this interval. All the stations tracking Lageos were permitted to adjust and compare to another set of stations derived from a set of polar motion data which was assumed to be perfect. The polar motion error which was imposed on the recovery contained both long and short period errors with a high frequency noise-like contribution also considered. These errors had an RMS systematic offset from the "true" polar motion of about 15 cm with a noise level of the order of 10 cm. The errors in UT1 were quite similiar. Since this solution was made using the actual contributions from each participating station, the experiment included stations which have been "fixed" over a good deal of the lifetime of Lageos--our so-called "base" stations--with other sites having more limited data or transitory occupancies. Therefore, the effect of the averaging of these errors over the tracking periods of individual sites was also assessed.

SIGNIFICANCE

The SLR technology is capable of relating sites even though they may have different tracking intervals with respect to one another. These site positions are tied together primarily through the rigor of the tracking network comprising the "base" stations but they also require proper earth orientation. When imposing a fixed polar motion and earth rotation rate error within this system, the rigor (geometric strength) of the network is tested against the misalignment of the network with respect to the orbital plane used as a reference frame.

Figure 1 shows the errors in baselines that occurred as a result of our perturbing both the pole and universal time from their true value by about 15 cm, as described earlier. In general, the numbers range from zero to a maximum of 5 cm and show that for the lines connecting our "base stations" the earth orientation errors are very small, 1 cm or less. Figure 2 shows the standard deviations of the baselines. Generally, these standard deviations are comparable to the changes in baseline length shown in Figure 1. The larger errors in Figure 1 and the larger s.d.s in Figure 2 generally correspond to the stations that had a minimum data set. For example, station 7896 (Pasadena) was only occupied for effectively about 6 weeks in late 1980 and during this time the global network was weaker than normal. This combination of a relatively short stay on site, coupled with a weak supporting network provides noticeably weaker baselines that are much more sensitive to error in the orbit and models.

We believe that the following simple relationship between systematic errors in earth orientation and the effect of these errors on baseline accuracies (σ) summarizes our results:

Baseline change (error) $\sim\sigma$ /20 x earth orientation error.

This expression implies that a 10 cm error in earth orientation (pole or U.T.) corrupts a strongly determined baseline (σ = 2 cm) by about 1 cm; and weakly determined baseline (σ = 5 cm) by about 2 to 3 cm.

The conclusion that we draw from this brief analysis is that baselines between stations that are supported by a global network of tracking stations are only marginally affected by errors in earth orientation. It appears that the global network of stations retains its integrity even in the presence of systematic changes in the coordinate frame, and minimizes the effect of these coordinate frame changes on the relative locations of the stations, i.e., baselines are not significantly affected.

STN	HT	7	7	7	7	7	7	7	7	7	7	7	7	7	7	7	7	7	7	7	7	7	7	7	7	7	7	
		0	0	0	0	0	0	0	0	0	1	1	1	1	1	1	1	1	1	2	8	8	8	8	8	9	9	9	9	
		5	6	6	8	8	9	9	9	9	0	0	0	0	1	1	1	1	2	1	3	3	3	9	9	0	2	2	4	
		1	2	3	2	6	0	1	2	6	2	3	5	9	0	2	4	5	0	0	3	4	5	2	6	7	1	9	3	
7051	0	0	0	1	2	-2	0	0	1	0	1	0	1	0	0	1	-1	-1	0	0	0	0	2	0	0	0	0	0	-1	QUINCY, CA
7062	0	0	0	0	0	-2	0	-1	1	1	0	0	0	0	0	0	0	1	0	0	0	0	0	-1	0	0	0	-1	-1	OTAY, CA
7063	0	1	0	0	-1	0	0	0	1	1	0	1	0	0	0	0	2	0	0	0	0	-1	0	0	4	0	1	0	0	GREENBELT, MD
7082	0	2	0	-1	0	-3	0	-2	2	1	0	-2	-1	1	0	0	2	0	0	1	-1	-1	0	0	4	-1	0	-2	-1	BEAR LAKE, UT
7086	0	-2	-2	0	-3	0	0	0	0	0	1	0	1	-2	-3	-2	0	-1	-1	-2	-1	-1	0	-3	0	2	-2	1	-1	FORT DAVIS, TX
7090	0	0	0	0	0	0	0	0	-1	-1	-1	-2	-1	0	0	0	0	0	0	0	0	0	-1	0	0	-1	0	-1	0	YARRAGADEE, AUS
7091	1	0	-1	0	-2	0	0	0	0	0	0	0	0	-1	-1	-1	0	0	-1	-1	-1	-1	0	0	3	3	0	2	0	WESTFORD, MA
7092	0	1	1	1	2	0	-1	0	0	0	0	-1	0	0	2	1	0	1	0	2	-1	0	0	0	0	0	2	-1	-2	KWAJELEIN
7096	0	0	1	1	1	0	-1	0	0	0	1	0	0	0	1	1	0	1	2	0	0	0	0	0	-1	0	1	-1	-2	AM. SAMOA
7102	0	1	0	0	0	1	-1	0	0	1	0	0	0	1	0	0	2	1	0	0	-2	-2	-1	1	4	0	2	-1	-1	GREENBELT, MD
7103	-2	0	0	1	-2	0	-2	0	-1	0	0	0	1	0	-1	-1	1	0	-1	-1	-2	-3	-1	0	3	0	0	0	-3	GREENBELT, MD
7105	0	1	0	0	-1	1	-1	0	0	0	0	1	0	0	0	0	2	0	0	0	-1	-2	0	1	4	0	1	-1	-1	GREENBELT, MD
7109	0	0	0	0	1	-2	0	-1	0	0	1	0	0	0	0	1	0	0	0	0	-1	0	1	0	1	0	1	0	-1	QUINCY, CA
7110	0	0	0	0	0	-3	0	-1	2	1	0	-1	0	0	0	0	1	1	1	0	-1	-1	0	-2	1	-1	0	-1	0	MONUMENT PEAK, CA
7112	0	1	0	0	0	-2	0	-1	1	1	0	-1	0	1	0	0	2	0	0	0	-1	-1	0	1	4	-1	1	-1	-1	PLATTEVILLE, CO
7114	1	-1	0	2	2	0	0	0	0	0	2	1	2	0	1	-2	0	0	-1	-1	0	0	2	0	2	1	2	1	-1	OWENS VALLEY, CA
7115	1	-1	1	0	0	-1	0	0	1	1	1	0	0	0	1	0	0	0	0	0	0	0	1	-1	4	1	1	0	0	GOLDSTONE, CA
7120	0	0	0	0	0	-1	0	-1	0	2	0	-1	0	0	1	0	-1	0	0	3	-2	-1	0	-1	-2	0	0	0	-1	MT. HALEAKALA, HI
7210	0	0	0	0	1	-2	0	-1	2	0	0	-1	0	0	0	0	-1	0	3	0	0	0	0	-1	-3	-1	0	-1	-1	MT. HALEAKALA, HI
7833	1	0	0	0	-1	-1	0	-1	-1	0	-2	-2	-1	-1	-1	-1	0	0	-2	0	0	0	5	0	2	1	0	2	0	KOOTWIJK, NETH
7834	0	0	0	-1	-1	-1	0	-1	0	0	-2	-3	-2	0	-1	-1	0	0	-1	0	0	0	1	0	2	-1	0	0	-1	WETTZEL, W. GERM.
7835	0	2	0	0	0	0	-1	0	0	0	-1	-1	0	1	0	0	2	1	0	0	5	1	0	2	4	-1	2	-1	-1	GRASSE, FRANCE
7892	0	0	-1	0	0	-3	0	0	0	0	1	0	1	0	-2	1	0	-1	-1	-1	0	0	2	0	2	-1	0	0	-1	VERNAL, UT
7896	1	0	0	4	4	0	0	3	0	-1	4	3	4	1	1	4	2	4	-2	-3	2	2	4	2	0	1	2	1	-2	PASADENA, CA
7907	0	0	0	0	-1	2	-1	3	0	0	0	0	0	0	-1	-1	1	1	0	-1	1	-1	-1	-1	1	0	0	0	-1	AREQUIPA, PERU
7921	1	0	0	1	0	-2	0	0	2	1	2	0	1	1	0	1	2	1	0	0	0	0	2	0	2	0	0	0	0	MT. HOPKINS, AZ
7929	0	0	-1	0	-2	1	-1	2	-1	-1	-1	0	-1	0	-1	-1	1	0	0	-1	2	0	-1	0	1	0	0	0	-1	NATAL, BRAZIL
7943	-1	-1	-1	-1	0	-1	-1	0	0	-2	-2	-1	-3	-1	-1	0	-1	-1	0	-1	-1	0	-1	-1	-1	-1	-2	-1	0	-1	0	ORRORAL, AUS.

Figure 1. Baseline Error Sensitivity to Earth Orientation.

STN	HT	7 0 5 1	7 0 6 2	7 0 6 3	7 0 8 2	7 0 8 6	7 0 9 0	7 0 9 1	7 0 9 2	7 0 9 6	7 1 0 2	7 1 0 3	7 1 0 5	7 1 0 9	7 1 1 0	7 1 1 2	7 1 1 4	7 1 1 5	7 1 2 0	7 2 1 0	7 8 3 3	7 8 3 4	7 8 3 5	7 8 9 2	7 9 0 6	7 9 2 7	7 9 2 1	7 9 4 3	
7051	.	0	3	2	3	3	2	2	4	3	2	4	2	2	3	2	3	3	2	2	4	4	3	3	4	2	3	2	2	QUINCY, CA
7062	.	3	0	2	4	2	1	2	4	3	2	4	2	3	2	2	3	3	2	2	3	4	3	4	4	2	2	2	2	OTAY, CA
7063	.	2	2	0	3	2	1	2	3	2	2	4	2	2	2	2	2	2	2	2	3	3	2	3	3	1	2	2	1	GREENBELT, MD
7082	.	3	4	3	0	3	2	3	4	3	3	4	3	3	3	3	3	3	3	3	4	4	3	4	4	2	4	3	2	BEAR LAKE, UT
7086	.	3	2	2	3	0	1	2	3	3	2	4	2	2	2	2	2	2	2	2	3	4	3	4	3	2	2	2	2	FORT DAVIS, TX
7090	.	2	1	1	2	1	0	1	4	3	1	3	1	1	1	1	1	1	1	1	2	2	2	3	3	1	1	1	2	YARRAGADEE, AUS
7091	.	2	2	2	3	2	1	0	3	2	2	4	2	2	2	2	2	2	2	2	3	3	3	3	3	1	2	3	1	WESTFORD, MA
7092	.	4	4	3	4	3	4	3	0	5	3	4	3	3	3	3	3	3	4	4	4	4	3	4	4	2	3	2	4	KWAJELEIN
7096	.	3	3	2	3	3	3	2	5	0	3	4	2	3	3	3	3	3	3	3	3	3	2	4	4	2	3	2	3	AM. SAMOA
7102	.	2	2	2	3	2	1	2	3	3	0	4	2	2	2	2	2	2	2	2	3	4	3	3	3	2	2	3	1	GREENBELT, MD
7103	.	4	4	4	4	4	3	4	4	4	4	0	4	4	4	4	4	4	3	4	4	5	4	4	4	4	4	4	3	GREENBELT, MD
7105	.	2	2	2	3	2	1	2	3	2	2	4	0	2	2	2	2	2	2	2	2	3	2	3	3	1	2	2	1	GREENBELT, MD
7109	.	2	3	2	3	2	1	2	3	3	2	4	2	0	2	2	2	2	2	2	3	4	3	3	4	1	2	2	1	QUINCY, CA
7110	.	3	2	2	3	2	1	2	3	3	2	4	2	2	0	2	2	2	2	2	3	4	2	3	3	1	2	2	1	MONUMENT PEAK, CA
7112	.	2	2	2	3	2	1	2	3	3	2	4	2	2	2	0	2	2	2	2	3	4	3	3	3	1	2	2	1	PLATTEVILLE, CO
7114	.	3	3	2	3	2	1	2	3	3	2	4	2	2	2	2	0	2	2	2	3	4	3	3	4	1	2	2	1	OWENS VALLEY, CA
7115	.	3	3	2	3	2	1	2	3	3	2	4	2	2	2	2	2	0	2	2	3	4	2	3	3	1	2	2	1	GOLDSTONE, CA
7120	.	2	2	2	3	2	1	2	4	3	2	3	2	2	2	2	2	2	0	2	3	3	2	3	3	1	2	2	1	MT. HALEAKALA, HI
7210	.	2	2	2	3	2	1	2	4	3	2	4	2	2	2	2	2	2	2	0	3	3	2	3	3	1	2	2	2	MT. HALEAKALA, HI
7833	.	4	3	3	4	3	2	3	4	3	3	4	2	3	3	3	3	3	3	3	0	5	5	4	4	2	3	4	2	KOOTWIJK, NETH
7834	.	4	4	3	4	4	2	3	4	3	4	5	3	4	4	4	4	4	3	3	5	0	5	5	4	2	4	4	2	WETTZEL, W. GERM.
7835	.	3	3	2	3	3	2	3	3	2	3	4	2	3	2	3	3	2	2	2	5	5	0	4	4	2	2	3	2	GRASSE, FRANCE
7892	.	3	4	3	4	4	3	3	4	4	3	4	3	3	3	3	3	3	3	3	4	5	4	0	4	3	4	3	3	VERNAL, UT
7896	.	4	4	3	4	3	3	3	4	4	3	4	3	4	3	3	4	3	3	3	4	4	4	4	0	3	3	3	3	PASADENA, CA
7907	.	2	2	1	2	2	1	1	2	2	2	4	1	1	1	1	1	1	1	1	2	2	2	3	3	0	1	2	1	AREQUIPA, PERU
7921	.	3	2	2	4	2	1	2	3	3	2	4	2	2	2	2	2	2	2	2	3	4	2	4	3	1	0	2	1	MT. HOPKINS, AZ
7929	.	2	2	2	3	2	1	3	2	2	3	4	2	2	2	2	2	2	2	2	4	4	3	3	3	2	2	0	2	NATAL, BRAZIL
7943	.	2	2	1	2	2	2	1	4	3	1	3	1	1	1	1	1	1	1	2	2	2	2	3	3	1	1	2	0	ORRORAL, AUS.

Figure 2. Estimate Baseline Uncertainty

OMIT

CHAPTER 2

GLOBAL EARTH DYNAMICS

OVERVIEW

Studies of global earth dynamics are devoted to improving the understanding of the origin of motions of the whole earth and determining the structural and mechanical properties of the earth's interior. The techniques employed in such studies are as varied as the studies themselves. They range from determination of changes in satellite orbits, to spectrum analyses of polar motion data, to studies of the flexural strength of the lithosphere.

1) The first report focuses on the analysis of the earth's rotation and compares the observations with the atmospheric and seismic excitation functions.

2) The second report continues the study of polar motion. It focuses on recent studies which will contribute towards the understanding of the excitation mechanism of the Chandler wobble.

3) The third report discusses the use of SEASAT altimeter data to obtain information about the flexural strength of the lithosphere.

4) The fourth report discusses modeling the perturbative force due to radiation pressure which acts on the orbit of Lageos.

5) The fifth report continues the assessment of the perturbative force due to radiation pressure which acts on the orbit of Lageos. In this latter report however, the diminuation of radiation pressure occurring when the Lageos satellite moves into the moon's shadow is assessed.

Contributors to this chapter are B.F. Chao, R. Gross, D.C. McAdoo*, and D.P. Rubincam.

* D.C. McAdoo now is with National Oceanic and Atmospheric Administration; National Geodetic Survey.

D7 N84 30462

ANALYSIS OF THE EARTH'S VARIABLE ROTATION

B. Fong Chao

OBJECTIVE

To analyze the Earth's rotation, and to compare the observations with the atmospheric and seismic excitation functions.

BACKGROUND

The variation in the Earth's rotation can be separated into the length-of-day (LOD) variation (the axial, or z-component) and the polar motion (the x-y component) (Munk & MacDonald, 1960). Possible driving mechanisms include: atmospheric/oceanic circulations, seismic activities, solar-lunar tides, mantle convection, core-mantle coupling, and solar activities (see e.g., Lambeck, 1980). The major problem of concern here is the identification of these dynamical processes as primary driving mechanisms for the various features in the variation of the Earth's rotation.

Besides the solar-lunar tidal terms, the LOD variation can be conveniently divided into frequency bands: (1) seasonal and short-period (time scale shorter than 1 year, including the dominant annual and semi-annual components), (2) interannual (1 to 10 years), and (3) decade and secular (longer than 10 years). The driving mechanism for (1) has recently been confirmed to be the changes in the atmospheric angular momentum by Rosen & Salstein (1983), while (2) and (3) have remained largely unstudied.

The polar motion is composed of the annual wobble, the 14-month Chandler wobble and a secular drift. It has been known (Wahr, 1983) that the energy associated with the atmospheric mass movement is sufficient to excite the observed annual wobble, although a time-domain correlation study is left to be desired. As for the Chandler wobble, despite a great deal of effort by various investigators over several decades, the primary driving mechanism is still a mystery. The latter is also true for the secular drift.

The data analysis procedures for the LOD and the polar motion are different. This is simply because the Earth's responses for the LOD and the polar motion differ in a fundamental way. For LOD, the solid Earth acts as an all-pass filter in the sense that whatever befalls it, it responds accordingly. This allows us to do a direct comparison of the LOD with excitation functions. For the polar motion, on the other hand, the Earth is a free oscillating system with a natural period of 14 months (the Chandler wobble). The transfer function of such a system has a peak at the natural

period and a phase delay of 90°. Therefore, prior to any comparison of polar motion observations with excitation functions, it is necessary to deconvolve the observed polar motion--a procedure often beset by noise.

RECENT ACCOMPLISHMENTS AND SIGNIFICANCE

For LOD, an empirial correlation study was conducted (Chao, 1984a) between the LOD variation and the southern oscillation (SO)/El Nino, the most prominent signal in interannual, global-scale atmospheric fluctuation characterized by a seesawing of air mass between eastern and western hemisphere in the tropical Pacific-Indian Ocean region. Indeed, any atmospheric mass movement, such as SO, that exerts an external torque on the solid-Earth will certainly induce LOD variations. Thus, two relevant time series for the period 1957-1983 were compared: the SO Index and the interannual LOD variation. The latter is obtained by removing the least-squares estimates for the long-period (secular and decade) and the seasonal variations in the BIH (Bureau Internationl de l'Heure) LOD series. The two series have a very encouraging qualitative correlation, in particular with respect to El Nino events (especially for the strong 1982-83 episode); and the linear correlation coefficient is found to be 0.55. It is believed that much, if not most, interannual LOD is caused by the SO, and the true correlation is considerably higher than its apparent value considering the fact that the SO Index is merely an indicator derived from two local atmospheric measurements while the LOD is a global quantity.

A comprehensive experimental study of the predictability of the polar motion was completed (Chao, 1984b) using a homogeneous BIH data set for the period 1967-1983. The numerical prediction of the Earth's polar motion is of both theoretical and practical interests. Thus, based on a general knowledge of the physics of the annual and the Chandler wobbles, a numerical model for the polar motion was built by allowing the wobble periods to vary. Using an optimum base length of 6 years for prediction, this "floating-period" model, equipped with a nonlinear least-squares estimator, is found to yield polar motion predictions accurate to within 0".012 to 0".024 depending on the prediction length up to one year, corresponding to a predictability of 91-83%. This represents a considerable improvement over the conventional fixed-period predictor, which, by its nature, does not respond to variations in the apparent wobble periods (in particular, a dramatic decrease in the periods of both the annual and the Chandler wobbles after the year 1980). The superiority of the floating-period predictor to other predictors based on critically different numerical models is also demonstrated.

On the theoretical front, a study was conducted (Chao, 1984c) on the maximum entropy/autoregressive (ME/AR) modeling of time series, a spectral method widely used in geophysics and, in particular, the study of the period and damping of the Chandler wobble. Thus, the AR model of a random process is interpreted in the light of the Prony's relation which relates a complex conjugate pair of poles of the AR process on the z-plane (or the z-domain) on the one hand, to the complex frequency of one complex harmonic function in the time domain on the other. It is then seen that the AR model of a time series is one that models the time series as a linear combination of complex harmonic functions, which include pure sinusoids and real exponentials as special cases. An AR model is completely determined by its z-domain pole configuration. The ME/AR spectrum, defined on the unit circle of the z-plane (or the frequency domain), is nothing but a convenient, but ambiguous visual representation. The position and shape of a spectral peak is determined by the corresponding complex frequency, and the height or area of the spectral peak contains little information about the amplitude of the complex harmonic functions.

FUTURE EMPHASIS

The Southern Oscillation (SO)-LOD correlation suggests that the atmospheric/oceanic mass transport associated with SO may also excite polar motion. In particular, the El Nino events do have a time scale close to the natural period of the Earth's wobble--the 14-month Chandler period. Unless the SO is essentially all equatorial, this means an observable signature in the Chandler wobble excitation function, which can be derived from the observed polar motion time series. A preliminary study using Lageos (LAser GEOdynamics Satellite) derived data has shown an encouraging correlation between the SO Index and the y-component of the polar motion excitation function (Gross and Chao, 1984).

REFERENCES

Chao, B.F., "Interannual Lenght-of-Day Variation with Relation to the Southern Oscillation/El Nino," in press Geophys. Res. Letters, 1984a.

Chao, B.F., "Predictability of the Earth's Polar Motion," submitted to J. Geophys. Res, 1984b.

Chao, B.F., "On the Maximum Entropy/Autoregressive Modeling of Time Series," NASA TM-86057, 1984c.

Gross, R.S., and B.F. Chao, "Excitation Study of the LAGEOS Derived Chandler Wobble," submitted to J. Geophys. Res., 1984.

Lambeck, K., The Earth's Variable Rotation, Cambridge Univ. Press, New York, 1980.

Munk, W.H., and G.J.F. MacDonald, The Rotation of the Earth, Cambridge Univ. Press, New York, 1960.

Rosen, R.D. and D.A. Salstein, "Variations in Atmospheric Angular Momentum on Global and Regional Scales and the Length-of-Day," J. Geophys. Res., 88, 5451-70, 1983.

Wahr, J.M., "The Effects of the Atmosphere and Oceans on the Earth's Wobble and on the Seasonal Variations in the Length-of-DayII, Results," Geophys. J. Roy. Astron. Soc., 74, 451-87, 1983.

Omit

THE OBSERVED EXCITATION FUNCTION OF THE CHANDLER WOBBLE

Richard Gross

OBJECTIVE

The objective of this research effort is to gain a better understanding of the mechanism that is keeping the Chandler wobble excited.

BACKGROUND

Any rigid body that is rotating about some axis which is not its principal moment of inertia axis will experience a wobble as it rotates. The rotation axis will oscillate about the inertia axis (as seen in a frame of reference attached to the rotating body) and will try to align itself with the inertia axis since their alignment represents a state of minimum energy for the rotating body. For the earth this motion is known as the Chandler wobble in honor of its discoverer. If the earth remained undisturbed during this motion, the rotation pole would trace a spiral about the inertia pole with a period of 434 days and an e-folding time for the amplitude decay of about 40 years. Eventually the motion would damp out entirely and the rotation and inertia axes would be aligned. However, the Chandler wobble has been under observation for the past 80 years and is seen to actually grow in amplitude during part of this time. Therefore, there must be some as yet unknown mechanism that is exciting the Chandler wobble. Any mechanism that causes mass motions of the earth on time scales much less than 434 days can be the source of this excitation. Amongst those proposed are earthquakes, weather effects and core-mantle interactions.

RECENT ACCOMPLISHMENTS

The equation relating the position of the rotation pole m to that of (essentially) the inertia pole Ψ is:

$$\Psi(t) = m(t) + \frac{i}{\sigma_0}\dot{m}(t)$$

where $m(t)$ is the complex-valued angular displacement of the rotation pole from the origin of some coordinate system, $\Psi(t)$ is the similar displacement for the inertia pole, σ_0 is the complex-valued eigenfrequency of the motion and the dot denotes time differentiation. This equation can be solved for $m(t)$ thereby obtaining:

$$m(t) = m_0 e^{i\sigma_0 t} - i\sigma_0 \int_0^t \Psi(t) e^{i\sigma_0 (t-\tau)} d\tau + n(t)$$

where m_0 is the initial position of the rotation pole and $n(t)$ represents the noise in the observed time series $m(t)$. By recognizing the above integral as a convolution, the problem of recovering $\Psi(t)$ from $m(t)$ is seen to be one of deconvolution. In this study $\Psi(t)$ is recovered by performing this deconvolution in the frequency domain modeling the noise as though it were white. The result is shown in figures 1 and 2.

SIGNIFICANCE

By correlating the features seen in this observed excitation function with known physical events on the earth (such as large earthquakes or strong El Nino/Southern Oscillation events) it should be possible to determine the source (or sources) of the excitation of the Chandler wobble.

FUTURE EMPHASIS

Continued interpretation of the excitation function derived from various observed Chandler wobble data sets is planned. If each and every wiggle in figures 1 and 2 can be physically explained then the question of the source of the excitation of the Chandler wobble will be solved.

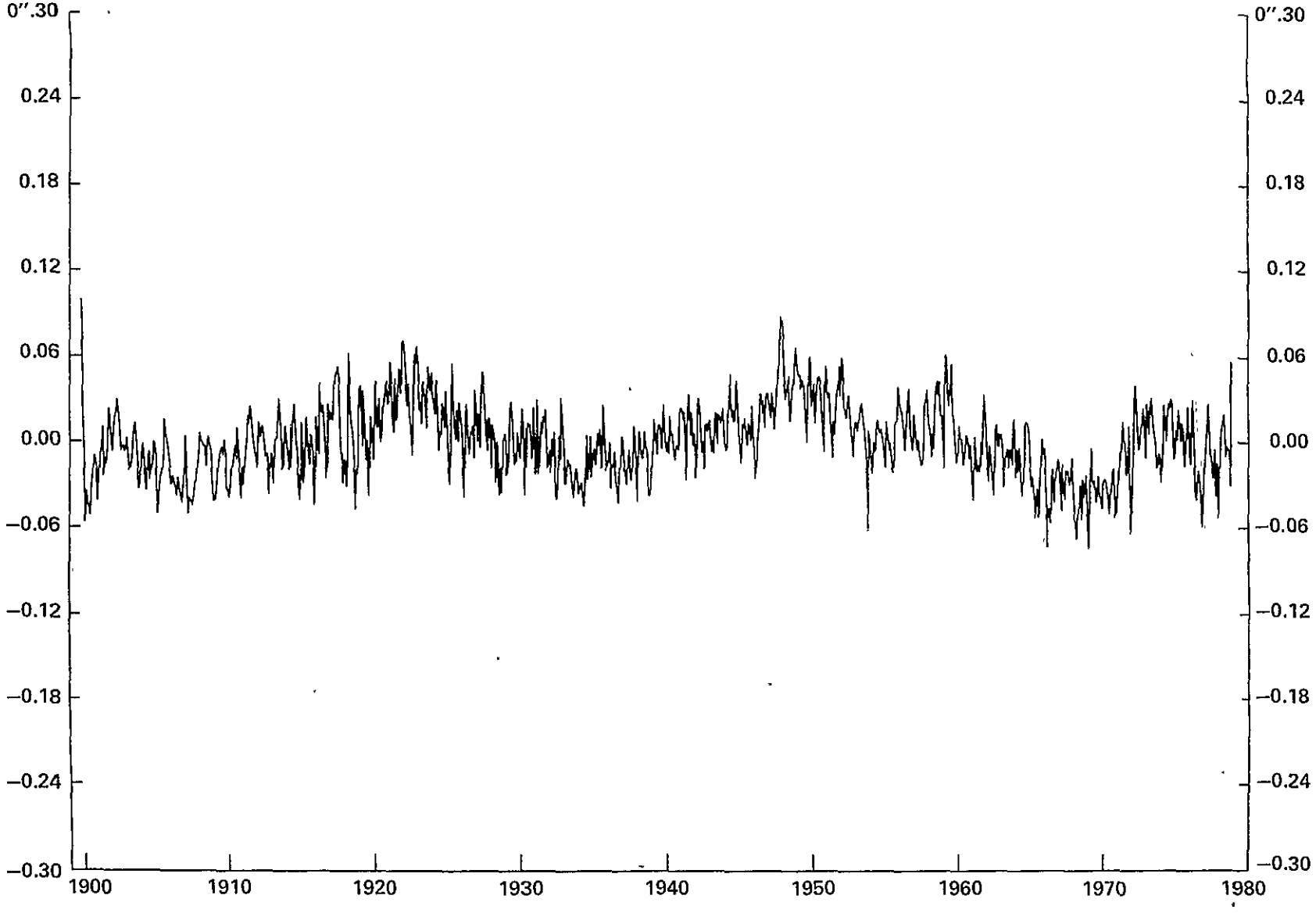

Figure 1. X-component of the Angular Displacement of the Excitation Axis from the CIO (Conventional International Origin).

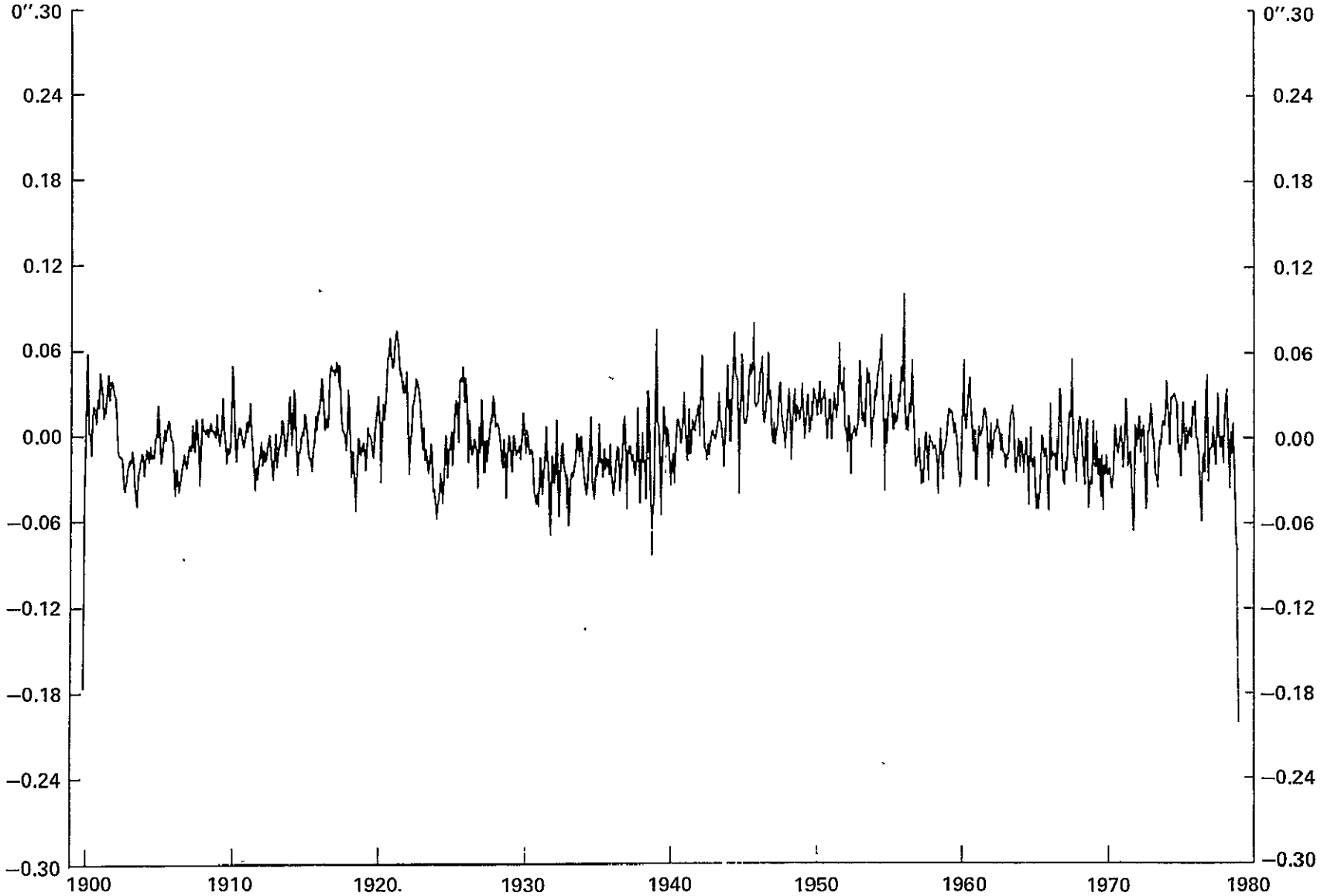

Figure 2. Y-component of the Angular Displacement of the Excitation Axis from the CIO (Conventional International Origin).

Dg

N84 30463

SEASAT OBSERVATIONS OF LITHOSPHERIC FLEXURE

David C. McAdoo

OBJECTIVE

In order to understand something about the dynamics of plate tectonics it is necessary to know how the lithosphere itself responds to tectonic forces. Specifically, we would like to estimate the flexural strength of the lithosphere. Further, we wish to describe the apparent dependence of this strength on age of lithosphere and magnitude of load.

BACKGROUND

Oceanic lithosphere of various ages is subjected to relatively large forces as it approaches subduction zones. Regions seaward of subduction zones are, in fact, uniquely suited to testing mechanical models of oceanic lithosphere. Outer Rises, represent the deformational response of the lithosphere to the forces in these regions. A substantial number of studies (see McNutt and Menard, 1982 or McAdoo and Martin, 1984, for references) have compared bathymetric observations of Outer Rises with models of lithospheric flexure. This study, which is now in its second year, has tested models of lithospheric flexure on SEASAT altimetric observations of the geoid over Outer Rises. These altimeter data have been found to provide significant new information about the strength of the oceanic lithosphere. Among the significant results derived from altimeter data is confirmation of the proposition that the effective elastic thickness, T_e, of the lithosphere increases with age in approximate accord with the relation $T_e \cong C \cdot age^{1/2}$. In fact, a study (McAdoo and Martin, 1984) of Outer Rises in six regions concludes that altimetric data provide better agreement with the age-thickness relation than do bathymetric data (see Figure 1). This thickness-age relation can be shown to agree with thermal models of the lithosphere when an experimentally-derived ductile flow law is invoked for rock comprising the lower lithosphere (Goetze and Evans, 1979). In fact, one can interpret effective elastic thickness as simply depth to a particular isotherm (~700°C).

RECENT ACCOMPLISHMENTS

The SEASAT study of Outer Rises in six regions--the Aleutian, Mariana, Izu-Bonin, Kuril, and Middle American trenches--has been accepted for publication (McAdoo and Martin, 1984). This study has now been extended to other regions including the Peru-Chile, Puerto Rico and Philippine trenches. To date, no bathymetric profiles across Outer Rises in these three regions have been analyzed. Therefore our altimetric results, shown in Figures 1 and 3, are novel. When our results for all nine regions are examined we conclude that the lithosphere does continue to strengthen out to 150 Myr--the approximate age of lithosphere being subducted at the Izu-Bonin and Mariana trenches. This conclusion contrasts strongly with that of McNutt and Menard (1982) who suggested that the lithosphere is weaker than predicted (Goetze and Evans, 1979) from experimental deformation of rocks. McNutt and Menard's work was based solely on bathymetric data. We find (McAdoo, et al., 1984) that the lithospheric rheology, or strength-depth envelopes, predicted by Goetze and Evans (1979) and later employed by Bodine et al. (1981) are consistent with the altimeter data. Figure 2 shows an idealized yield stress envelope for realistic rheology lithosphere (RRL) of two different ages, 60 Myr and 160 Myr.

Thermally activated creep in the ductile regime governs the shape of the envelope (and effective elastic thickness) at depth. A nominal strain rate of $10^{-6}s^{-1}$ is assumed. Activation energies for ductile flow are from Goetze and Evans. Brittle or cataclastic failure controls the envelope shape in the shallow regime. An elastic core separates the ductile and brittle zones; its thickness is load dependent. Using this realistic rheology as sketched in Figure 2, a maximum collapse moment can be calculated as a function of thickness or age. From the application of the elastic lithospheric model to SEASAT data we calculate a zero-crossing moment which closely approximates the actual maximum moment (see McNutt and Menard, 1982). Therefore, maximum moments from analysis of SEASAT data agree well with those predicted by rock mechanics experiments (RRL). In summary both the age vs. thickness relation and maximum moment vs. thickness relation predicted by rock mechanics experiments (RRL) agree with SEASAT altimeter observations.

SIGNIFICANCE

SEASAT altimeter data over Outer Rises provide an important constraint on mechanical models of the oceanic lithosphere. These data are quite consistent with an experimentally predicted mechanical model (RRL) of the lithosphere which indicates that this model may be useful in other geodynamic investigations.

FUTURE EMPHASIS

The potential utility of SEASAT and other satellite altimeter data for studying dynamics of the lithosphere and sub-lithosphere is only beginning to be exploited.

Similar studies based on SEASAT data will be attempted in intra-plate regions. For example, the lithospheric folding in the central Indian Ocean Basin can perhaps be explained using the realistic rheological (RRL) model of the lithosphere.

REFERENCES

Bodine, J.H., M.S. Steckler and A.B. Watts, "Observations of Flexure and of the Oceanic Lithosphere," J. Geophys. Res.., 86, 3695-3707, 1981.

Goetze, C., and B. Evans, "Stress and Temperature in the Bending Lithosphere as Constrained by Experimental Rock Mechanics," Geophys. J.R. astr. Soc., 59, 463-478, 1979.

McAdoo, D.C. and C.F. Martin, "SEASAT Observations of Lithospheric Flexure Seaward of Trenches," J. Geophys. Res., in press, 1984.

McAdoo, D.C., C.F. Martin and S. Poulose, "SEASAT Observations of Flexure: Evidence for a Strong Lithosphere," Abstract, Spring AGU Meeting, 1984.

McNutt, M.K. and H.W. Menard, "Constraints on Yield Strength in the Oceanic Lithosphere Derived from Observations of Flexure," Geophys. J.R. astr. Soc., 71, 363-394, 1982.

FIGURE CAPTIONS

Figure 1. Effective elastic thickness, T_e, derived from SEASAT data (crosses) over nine trenches. Results from Middle America (MD), Aleutian (A), Philippine (P), Kuril (K), Mariana (M), and Bonin (B), indicated by solid crosses. Results from Puerto Rico (PR), Peru (PC) and South Sandwich (S), indicated by dashed crosses, T_e's are plotted versus age. Bodine et al. (1981) age-thickness relation (9) is shown as curves; see text. Dots are estimates of T_e derived from ship bathymetric profiles by Caldwell (1978) for trenches M, MD, A and P, by Caldwell et al. (1976) for B and by McAdoo et al. (1978) for K.

Figure 2. Yield stress envelope (linearized) for lithosphere (RRL) of two different ages. Adapted from Goetze and Evans (1979). Strain rate $\dot{\epsilon} = 10^{-16} s^{-1}$ is assumed (Parsons).

Figure 3. Maximum moment, M_0, (actually zero-crossing moment) vs. lithospheric thickness as inferred from SEASAT data over 9 Outer Rises (see Figure 1). Curve represents prediction from lithospheric model (RRL).

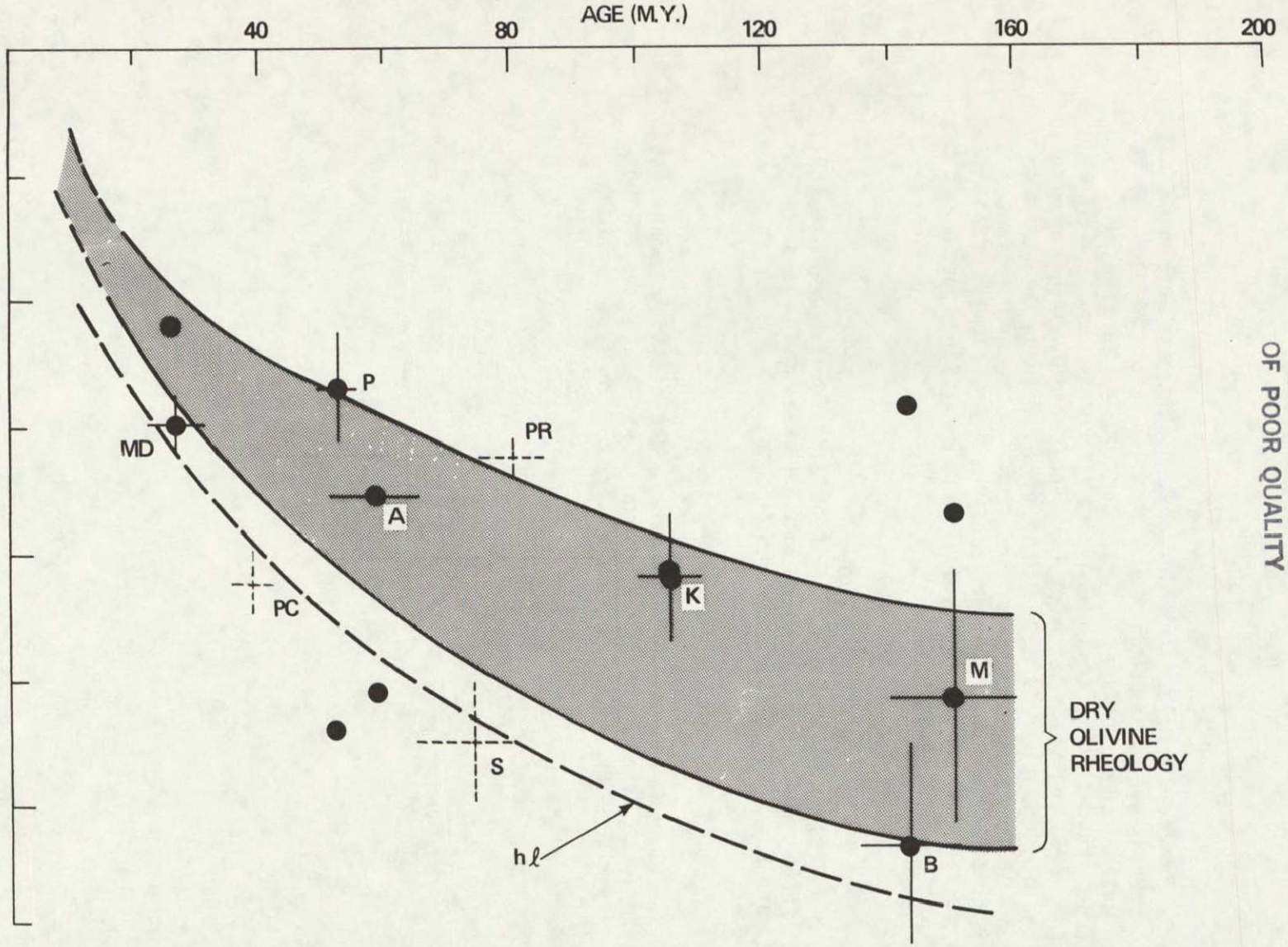

Figure 1. Effective Elastic Thickness, T_e, Derived from SEASAT Data (Crosses) Over Nine Trenches. Results from Middle America (MD), Aleutian (A), Philippine (P), Kuril (K), Mariana (M), and Bonin (B), Indicated by Solid Crosses. Results from Puerto Rico (PR), Peru (PC) and South Sandwich (S), Incidated by Dashed Crosses, T_e's are Plotted Versus Age. Bodine et al. (1981) Age-Thickness Relation (9) is Shown as Curves; See Text. Dots are Estimates of T_e Derived from Ship Bathymetric Profiles by Caldwell (1978) for Trenches M, MD, A and P, by Caldwell et al. (1976) for B and by McAdoo et al. (1978) for K.

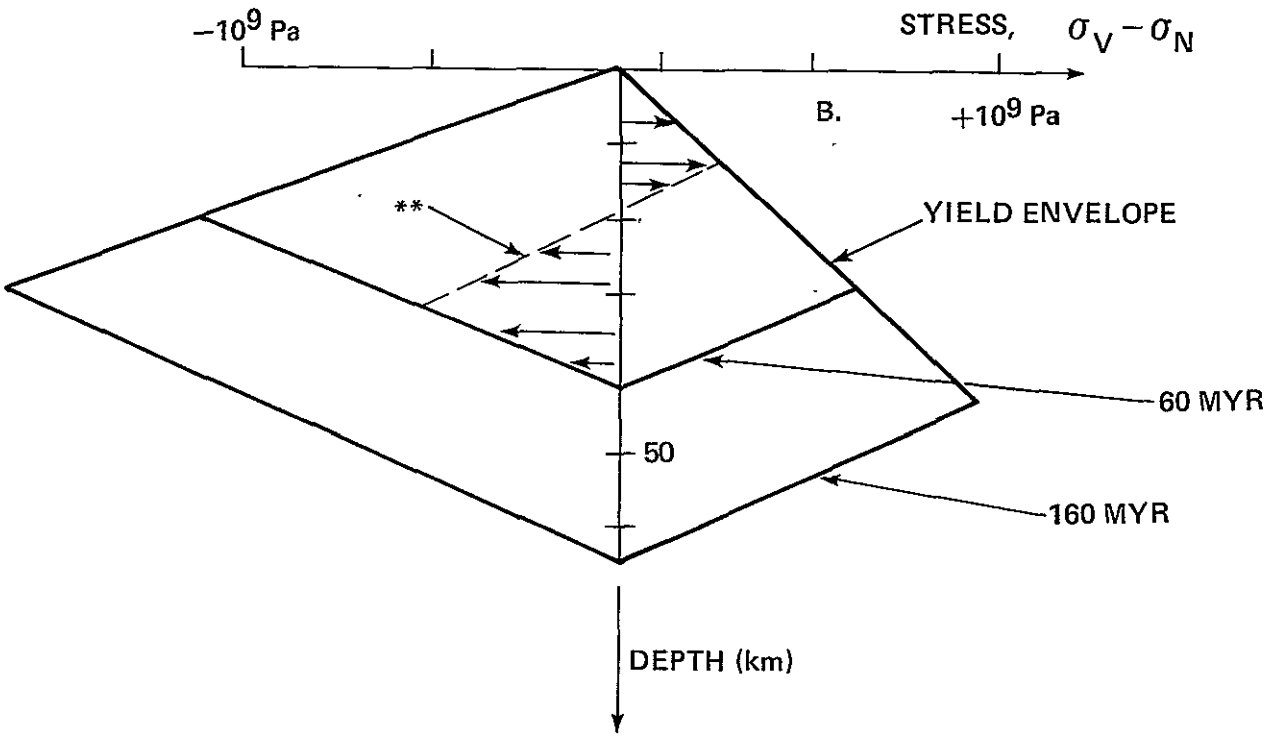

Figure 2. Yield Stress Envelope (Linearized) for Lithosphere (RRL) of Two Different Ages. Adapted from Goetze and Evans (1979). Strain Rate $\dot{\epsilon} = 10^{-16} s^{-1}$ is Assumed (Parsons).

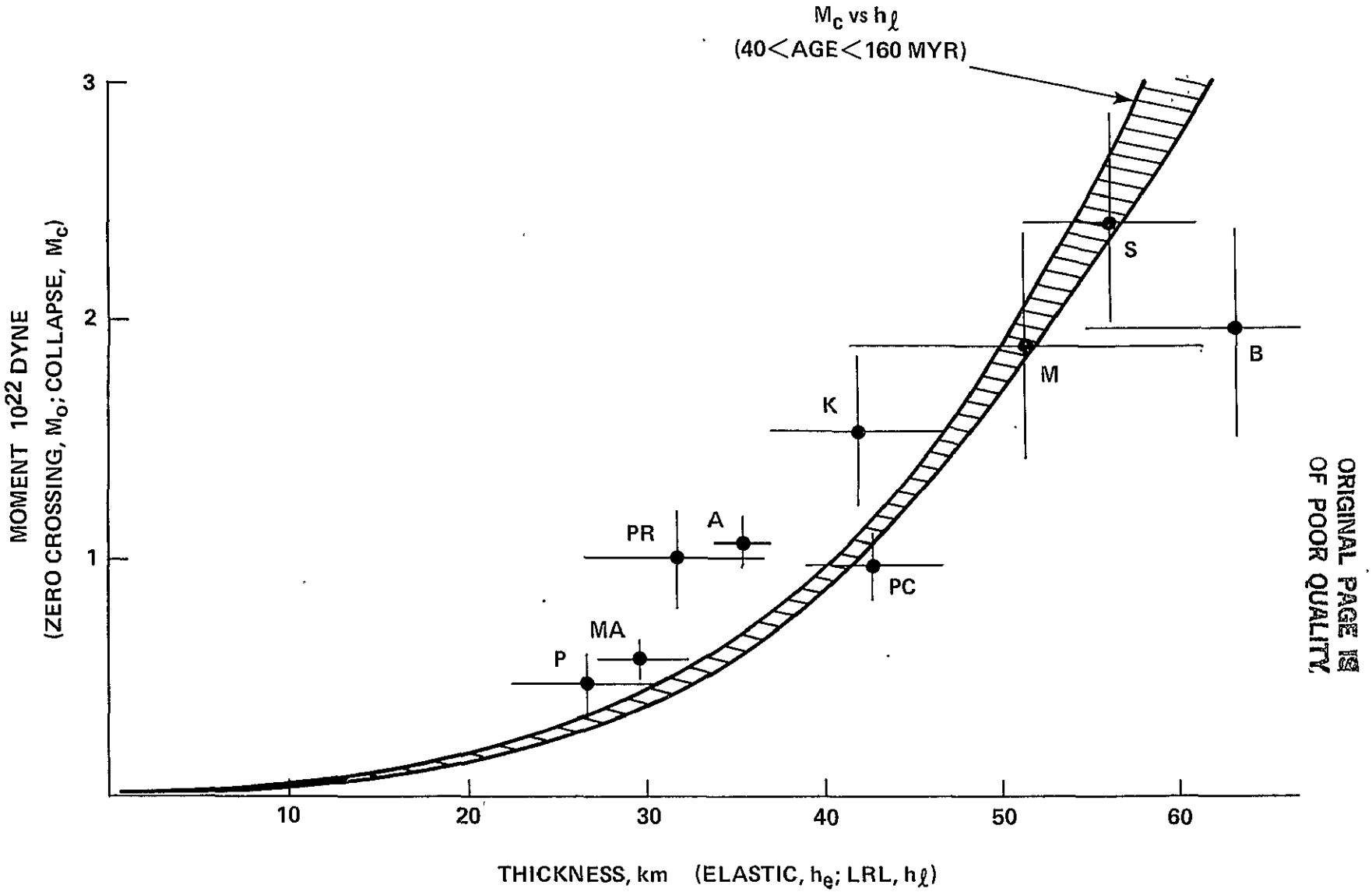

Figure 3. Maximum Moment, M_o, (Actually Zero-Crossing Moment) vs. Lithospheric Thickness as Inferred from SEASAT Data Over 9 Outer Rises (See Figure 1). Curve Represents Prediction from Lithospheric Model (RRL).

LAGEOS ORBIT AND THE ALBEDO PROBLEM

David P. Rubincam

OBJECTIVE

To obtain an analytic expression for the radiation pressure force on a satellite due to sunlight reflected from the earth. (This is commonly called the albedo problem).

BACKGROUND

The Lageos satellite undergoes unexplained along-track accelerations on the order of 3×10^{-12} ms^{-2}, once the average charged particle drag effect is removed. These accelerations are believed to be due mainly to terrestrial radiation pressure (Smith, 1983; Anselmo, et al., 1983). The effect of sunlight reflected off the surface of the earth must thus be modeled to insure an accurate orbit for Lageos. An accurate orbit is necessary for carrying out Lageos' mission of measuring tectonic plate motion, polar motion, and earth rotation.

An analytic expression for the force due to reflected sunlight is desirable to avoid a time-consuming numerical integration when computing the orbit. Obtaining such an analytic expression is a venerable problem in celestial mechanics (e.g., Lockry, 1966; Smith, 1970, and Lautman, 1977a, 1977b). Difficulties include integrating over only the sunlit portion of the earth seen by the satellite, assuming that the surface follows Lambert's law, and a geographically and temporally varying albedo.

RECENT ACCOMPLISHMENTS

The present investigation focuses on a spherical harmonic approach to the problem. An equation for the force has been obtained by assuming the earth's surface reflects sunlight according to Lambert's law. The equation is an integral over the whole earth's surface. Expressions occurring inside the integral are expressed in terms of spherical harmonics. The problem is thus reduced to integrating products of spherical harmonics.

FUTURE EMPHASIS

Future work will concentrate on working out the integration of the product of the spherical harmonics. The integration will give a sum of a large number of terms. The dominant terms for Lageos will be found and their effect on the orbit will be assessed.

REFERENCES

Anselmo, L., P. Farinella, A. Milani, and A.M. Nobili, "Effects of the Earth-Reflected Sunlight on the Orbit of the Lageos Satellite," Astron. Astrophys., 117, 3-8, 1983.

Lautman, D.A., "Perturbations of a Close-Earth Satellite Due to Sunlight Diffusely Reflected from the Earth. I. Uniform Albedo," Celest. Mech., 15, 387-420, 1977a.

Lautman, D.A., "Perturbations of a Close-Earth Satellite Due to Sunlight Diffusely Reflected from the Earth. II. Variable Albedo," Celest. Mech., 16, 3-25, 1977b.

Lochry, R.R., "The Perturbative Effects of Diffuse Radiations from the Earth and Moon on Close Satellites," Ph.D. Thesis, University of California at Los Angeles, 1966.

Smith, D.E., "Earth-Reflected Radiation Pressure," in Dynamics of Satellites (1969), COSPAR-IAU-IAG/IUGG-IUTAM Symposium, edited by B. Morando, pp. 284-294, Springer-Verlg, Berlin, 1970.

Smith, D.E., "Acceleration on Lageos Spacecraft," Nature, 304, 15, 1983.

LAGEOS ORBIT AND SOLAR ECLIPSES

David P. Rubincam

OBJECTIVE

To assess the importance of solar eclipses on Lageos' orbit.

BACKGROUND

Solar radiation pressure perturbs the orbit of the Lageos satellite. The GEODYN orbit determination computer program includes solar radiation pressure as one of the forces operating on the satellite as it integrates the orbit. GEODYN also takes into account the extinction of sunlight when Lageos moves into the earth's shadow.

GEODYN does not at present take into account the diminution of radiation pressure when Lageos moves into the moon's shadow, i.e., suffers a solar eclipse by entering the moon's umbra or penumbra. This diminution will affect Lageos' orbit by weakening for a time the radiation presure acting on the satellite. The importance of this effect must be assessed in order to assure an accurate integration of Lageos' orbit. An accurate orbit is necessary for Lageos to accomplish its mission of monitoring tectonic plate motion, polar motion, and earth rotation.

RECENT ACCOMPLISHMENTS AND SIGNIFICANCE

The effect of solar eclipses on the semimajor axis of Lageos' orbit has been computed analytically by assuming Lageos to be in a circular orbit, the sun and the moon to be in the plane of the orbit, and the moon to be stationary in the sky in front of the sun. Also, the magnitude of the radiation pressure is assumed to be linearly related to the angular separation of the sun and moon, and that Lageos is a perfect absorber of radiation.

The computation indicates that an eclipse of the sun by the moon as seen by Lageos can affect the semimajor axis at the 1 centimeter (1 cm) level. (On the time-scale of a day this will appear as an instantaneous change in the semimajor axis--an eclipse will last about an hour at most). Such a change is significant enough to include in GEODYN, in order to get an accurate orbit for Lageos.

FUTURE EMPHASIS

The task ahead is to determine just how often Lageos has been eclipsed in the past and how each eclipse affected the orbit. To do this, a computer program will be developed to look at the solar,

lunar, and Lageos positions around the time of each new moon since Lageos' launch. It will see if an eclipse took place, and if so, the perturbation of the orbit. About 20 penumbral and no umbral eclipses are expected.

CHAPTER 3

GRAVITY FIELD MODEL DEVELOPMENT

OVERVIEW

Knowledge of the earth's gravity field is fundamental to understanding the dynamics of the earth. For solid earth physics, knowledge of the variations in the gravity field provides information on the earth's physical properties and geodynamic processes and places constraints on the internal structure of the earth. In oceanography, knowledge of departure of the actual sea surface from a unique equipotential surface of the earth's gravity field (the geoid) can reveal information on oceanic circulation. In addition, other areas which benefit from knowledge of the earth's gravity field are satellite orbit determination and classical geodesy. This chapter describes:

1) The development and evaluation of a specialized gravity field model for Lageos which is used for the analysis of satellite laser ranging measurements and the accurate relative changes in these locations are used to study determination of tracking station locations of tectonic plate motion.

2) The developmental status of the Geodynamics Computational System (GEODYN)

   and

3) The development of ancillary computer software supporting geodynamic research in terms of error analysis and eigen-vector analysis.

Contributors to this chapter are F.J. Lerch, B.H. Putney, and T.L. Felsentreger.

D11

N84 30466

VERIFICATION OF THE ACCURACY OF GEM-L2 IN RESPONSE TO CRITICISM BY LAMBECK AND COLEMAN

Francis J. Lerch

OBJECTIVE

The objective is to evaluate the accuracy of GEM-L2 and its improvement in estimating Lageos orbits in order to provide better baselines for plate tectonics, improved polar motion and earth rotation. Analyses and comparisons with other models are made to verify our accuracy in contrast to the Lambeck and Coleman result which denied our accuracy estimates. Also the purpose of GEM-L2 is to improve the low degree and order geopotential which will provide for refinement of our knowledge of the broad features of ocean circulation.

BACKGROUND

The development of the gravity field for Lageos was a principal investigation in the Crustal Dynamics Project. Based upon the previous Goddard Earth Model, GEM 9, a global set of baselines (Table 1) were improved from 7 cm with this model to 1.8 cm with the new GEM-L2 model. However, the accuracy (Table 2) of GEM-L2 was claimed in a recent publication by Lambeck and Coleman (1983) to be no better for the low degree terms than the differences with other existing models (GRIM 3, SAO 77). These differences, particularly degree 3 are an order of magnitude larger (Table 3) than the accuracy of GEM-L2. Evaluation and comparisons are made to dispute the Lambeck/Coleman claim and to show that their "error spectrum" estimate for models is highly unreliable.

RECENT ACCOMPLISHMENTS

A refined gravity field model, Goddard Earth Model GEM-L2 (Lerch, et al.), has been derived using the Lageos orbital data yielding better baseline measurements (Table 1) for the analysis of tectonic plate motion. This field also contributes to a better understanding of the broad features of ocean circulation through its improvement of the long wavelength geoid (terms through degree and order 4) with an accuracy estimated at ± 8 cm (Table 2). In GEM-L2 two and half years of Lageos laser data acquired from over 20 well-distributed stations were combined with the existing data from the best satellite-derived model, GEM-9 (Lerch, et al.). The accuracy estimates of GEM-L2 are verified below.

First the general accuracy of the model is reviewed from an evaluation based upon new gravity anomaly data (Table 4). Letting the symbol <x> denote an average value of x over the earth Kaula's formula (1966), namely

$$\text{EST } \sigma^2 D_{ATA}(\Delta g_S) = \langle \Delta g_S^2 \rangle - \langle \Delta g_S \Delta g \rangle$$

was used as a test criteria to estimate the accuracy (commission error) of the gravity anomaly (Δ_S) of a satellite model from a global distribution of gravity anomaly data (Δ). The gravity anomaly error in GEM-L2 may be computed from the coefficient errors as follows:

$$\sigma^2_{\text{GEM-L2}}(\Delta g_S) = \gamma^2 \sum_{n=2}^{N} \sum_{m=0}^{n} (n-1)^2 \{\sigma^2(C_{\ell m}) + \sigma^2(S_{\ell m})\}$$

This error estimate is then compared in Table 4 with Kaula's test criteria above to verify the GEM-L2 error estimates using a number of gravity anomaly data sets. A calibration factor k is defined in the table and was employed to compare the agreement of the error estimates, namely

$$\text{EST } \sigma D_{ATA}(\Delta g_S) = k\sigma_{\text{GEM-L2}}(\Delta g_S)$$

The satellite σ has already been calibrated upward by a factor of $\sqrt{10}$ as previously done since the GEM-5 model (Lerch, et al., 1974) using the same method with surface gravity data only. The new gravity anomalies, using SEASAT over ocean areas and gravimetry over land areas, show that the errors in the satellite model are verified and in fact should be reduced by about one-third ($k \simeq .67$) from the previous estimate which was determined from the worldwide use of gravimetry only ($k = 1.0$). The improved set of gravity anomalies is responsible for the better calibration factor.

Since the gravity anomaly data are more sensitive to the higher degree terms, a test was made to estimate the calibration factor for the errors in the low degree terms to which Lambeck and Coleman primarily objected. In Table 5 independent solutions from optical data only and laser data only were used to calibrate the low degree error estimates for terms out through degree and order 10. As described in the table the coefficient differences are compared with satellite σ's for each degree ℓ. The result shows the same agreement from the calibration factor ($k \simeq .67$) as obtained from the new gravity anomaly data above in Table 4.

In Table 3 a comparison of the 3rd degree coefficient differences between GEM-L2 and the fields of SAO 77 and GRIM 3 verify the Lambeck/Coleman statement that these are an order of magnitude larger than the accuracy estiamtes of GEM-L2 in Table 2. However, a more recent European companion field to GRIM-3, namely GRIM-3B,

has an rms difference of 10 cm with GEM-L2 which is similar to GEM 9 as in Table 2. This result with GRIM-3B nullifies the argument that recent models from different institutions do not agree closely with one another.

A comparison for low degree terms between data on 24-hour satellites and different gravity models was obtained by Carl Wagner (1983) and presented in Table 6. These results support the accuracy of the GEM-L2 model and show that the large differences with the SAO and GRIM-3 models found above correspond to errors in these models rather than to GEM-L2.

It is now shown that the error spectra estimator of Lambeck and Coleman for terms of degree ℓ is highly unreliable. This is particularly so for low degree terms which they used to evaluate our fields (Tables 1,2,4,5, and 6 of their report). The estimator is given by (equation 8C of their report)

$$e_\ell^2 = C_\ell^2 - C_\ell \overline{C}_\ell$$

where C_ℓ is the field to be tested and $\overline{C}_\ell$ is a reference field, and where the vector C_ℓ denotes the spherical harmonic coefficients of degree ℓ and C_ℓ^2 the power in these terms. Using σ_ℓ^2 to denote the power of the coefficient errors of degree ℓ then the expected value of e_ℓ^2 (assuming the errors in C_ℓ and $\overline{C}_\ell$ are unbiased and uncorrelated) is

$$E(e_\ell^2) = \sigma_\ell^2 = \sum_{m=0}^{\ell} [\sigma^2(C_{\ell m}) + \sigma^2 (S_{\ell m})]$$

Hence the estimator is unbiased.

The variance of the estimator represents the spread or deviation of the estimator from its expected value, namely

$$\sigma^2(e_\ell^2) = E[e_\ell^2 - E(e_\ell^2)]^2$$

It is used to measure the reliability of the estimator e_ℓ^2, i.e., if $\sigma^2(e_\ell^2) \gg e_\ell^2$ the estimator is significantly unreliable and if $\sigma^2(e_\ell^2) < e_\ell^2$ it is considered a good estimator.

A simplified case can be used to test the estimator. Let individual errors in the coefficients of degree ℓ in the test field be normally distributed with equal variances ($\sigma^2 = \sigma_\ell^2/2\ell+1$) and let the power in individual coefficients be given by Kaula's rule ($k_\ell^2 = 10^{-10}/\ell^4$). Then the predicted error spread is given by

$$\sigma^2(e_\ell^2) = \frac{2}{2\ell+1} \sigma_\ell^4 + (\sigma_\ell^2 + \sigma_\ell^2) K_\ell^2 + \frac{\sigma_\ell^2 \sigma_\ell^{-2}}{2\ell+1}$$

where $\bar{\sigma}_\ell^2$ is the error power spectra for the reference field. Denoting the linear spread in the estimator as

$$\sigma(e_\ell) = [\sigma^2(e_\ell^2)]^{\frac{1}{4}}$$

a reliability factor for the estimator is given as follows

$$r = \frac{\sigma(e_\ell)}{\sigma_\ell}$$

where r denotes the root square error ratio of the variance of the estimator (e_ℓ^2) to the expected value (σ_ℓ^2) of the estimator.

Two cases are given in Table 7 to show the reliability r of the estimator:

$$r_0 = \frac{\sigma(e_\ell)}{\sigma_\ell} = [\frac{K_\ell^2}{\sigma_\ell^2} + \frac{2}{2\ell+1}]^{\frac{1}{4}} \qquad \text{for } \bar{\sigma}_\ell = 0$$

$$r_2 = [\frac{6}{2\ell+1} + \frac{5K_\ell^2}{\sigma_\ell^2}]^{\frac{1}{4}} \qquad \text{for } \bar{\sigma}_\ell = \sigma_\ell$$

For purposes of comparison with results from Lambeck and Coleman given in Table 6, the error spectra σ_ℓ are taken from GEM-L2. From inspection of the table this simplified statistical case for $r=r_2$ shows that the estimator significantly over estimates the errors in GEM-L2 by a factor of $r = 60$ for $\ell=2$ to $r = 9$ for $\ell=5$ and the predicted spread $\sigma(e_\ell)$ corresponds reasonably with the Lambeck/Coleman estimator. Hence the estimator essentially has no reliability for estimating the error power spectra of GEM-L2. Also note that even if the reference field is perfect ($\bar{\sigma}_\ell = 0$) the estimator has no reliability in the error spectra for $\ell = 2$ to 5 corresponding to the low degree terms.

The rms of laser residuals on Lageos arcs are presented in Table 8. The residuals of the SAO 77 field are an order of magnitude larger than GEM-L2 values. This serves to verify that the differences in the coefficients between GEM-L2 and SAO 77, which are an order of magnitude larger than the errors in GEM-L2 (see Tables 2 and 3), correspond to errors in the SAO field and not to those in GEM-L2 as claimed by Lambeck and Coleman. It is of further interest to note in Table 8 that GEM 9, which is independent of the Lageos data, does just as well with the Lageos orbital residuals as GRIM-3B and the University of Texas fields which employed this data in their solutions.

SIGNIFICANCE

The analysis presented here completely verifies the accuracy of the GEM-L2 model and disproves the statistical methods of Lambeck and Coleman rejecting the accuracy of GEM-L2 as published in their report. The baselines derived from Lageos with GEM-L2 have been estimated to have a 2 cm uncertainty due to the errors in the GEM-L2 gravity model which is supported by the results in Table 1. The calibration tests of this report indicate that the errors in GEM-L2 should be reduced by about 30 percent which is in the opposite direction to the result obtained by Lambeck and Coleman.

FUTURE EMPHASIS

Future work is continuing to improve the Crustal Dynamcis Gravity Model, GEM-L2, with more recent and accurate laser data. More extensive analyses verifying the accuracy of the GEM-L2 model will be published in a Special Lageos Issue of JGR.

REFERENCES

Kaula, W.M., "Tests and Combinations of Satellite Determinations of the Gravity Field," J. Geophys. Res., 71, 5303-5314, 1966.

Lambeck, K. and Coleman, R. (1983), "The Earth's Shape and Gravity Field: A Report of Progress from 1958 to 1982," Geophys. J.R. Astr. Soc. (1983), 74, pp. 25-54.

Lerch, F.J., C.A. Wagner, J.A. Richardson, J.E. Brownd, "Goddard Earth Models (5 and 6)," GSFC X-921-74-145, 1974.

Lerch, F.J., Klosko, S.M., R.E. Laubscher, C.A. Wagner, "Gravity Model Improvement Using GEOS-3 (GEM-9 and 10)," J. Geophys. Res., 84, (134) 3897-3915, 1979.

Lerch, F.J., S.M. Klosko, and G.B. Patel, "A Refined Gravity Model from LAGEOS (GEM-L2)," Geophys. Res. Lett., 1982.

Lerch, F.J., "Status of the Geopotential," Reviews of Geophysics and Space Physics, Vol. 21, No. 3, 560-565, 1983.

Lerch, F.J., S.M. Klosko, C.A. Wagner, and G.P. Patel, "On the Accuracy of Recent Goddard Gravity Models," J.Geophys. Res., (submitted).

Wagner, C.A., "The Accuracy of Low-Degree Geoptential: Implications for Ocean Dynamics," J. Geophys. Res., 88, B6, 5083-5090, 1983.

Table 1
Baseline Comparison from Two Independent Lageos Data Sets
Spanning 1979 Through 1980*

	GEM-9		GEM-L2		
	w/BIH** Polar Motion and A1-UT1	w/LAGEOS Polar Motion and A1-UT1	w/BIH Polar Motion and A1-UT1	w/LAGEOS Polar Motion & BIH A1-UT1	w/LAGEOS Polar Motion and A1-UT1
Baseline Agreement for Eight "Base" Stations (All 28 Baselines)	7.2 cm	6.0 cm	6.9 cm	4.7 cm	1.8 cm
"Base" Stations are:	7063 GSFC, MD 7086 Ft. Davis, Texas 7090 Yarragadee, Australia 7091 Westford, MA 7115 Goldstone, CA 7114 Owens Valley, CA 7907 Arequipa, Peru 7943 Orroral, Australia				

*The data has been divided into alternating 15 day segments and therefore both solutions have similar and uniform data distribution from these sites.

**BIH circular D 90-day smoothed values.

Table 2
Estimated Individual Low Degree and Order Coefficient Accuracy (cm)

COEFFICIENT	UNCERTAINTY GEM–9	UNCERTAINTY GEM–L2	ACTUAL COEFFICIENT DIFFERENCE (GEM–9) MINUS (GEM–L2)	
(ℓ, m)	$\sigma J_{\ell, m}$	$\sigma J_{\ell, m}$	ΔC	ΔS
C2,0	0.4	0.3	– .3	
C3.0	1.0	0.1	.5	
C4,0	0.8	0.7	.2	
C,S2,1	2.3	1.3	.5	.6
2,2	3.1	0.9	– 2.5	.9
3,1	4.8	2.3	– .4	1.-
3,2	7.2	3.4	– 7.7	– 4.1
3,3	8.6	3.2	–13.1	– 2.4
4,1	4.5	3.7	1.5	.8
4,2	4.4	3.3	– 1.3	1.2
4,3	4.1	2.4	– 3.0	– .3
4,4	5.6	2.4	– 2.9	– 5.1
TOTAL: RSS GEOID ACCURACY FOR				
4x4	15.9 cm	8.1 cm	17.7 cm	

GLOBAL 4 x 4 GEOID 2800 CM
PERCENT ACCURACY OF GEM–L2 = 0.3%

Table 3

Comparison of 3rd Degree Coefficients of Recent Gravity Fields with GEM-L2

	COEFF VALUES GEM-L2	COEFFICIENT DIFFERENCES (CM) (GEM-L2 - OTHER)				
	x 10^6	SAO 72	SAO 77	GRIM 2	GRIM 3	GRIM 3B
C3,0	0.958	– 1.5	– 1.5	– 1.9	– 0.6	–0.0
C3,1	2.029	20.0	–12.8	42.7	– 5.1	1.9
S	0.250	17.0	–17.2	60.5	1.3	1.3
C3,2	0.903	79.5	– 9.3	24.8	–50.6	–7.8
S	–0.616	88.8	41.5	–45.3	–57.8	–3.1
C3,3	0.722	148.0	36.2	6.4	13.4	–5.1
S	1.414	–72.7	–47.2	–91.2	–52.3	–3.1
RSS DIFFERENCE (CM		205.1	76.2	128.5	94.1	10.6

Table 4

Calibration of Satellite Model Errors

$$\text{EST } \sigma_{\text{Data}}\ (\Delta g_s) = k\,\sigma_{\text{Model}}\ (\Delta g_s) = k\sqrt{10}\ \sigma_{\text{Formal}}\ (\Delta g_s)$$

TEST CALIBRATION FACTOR $K = \sqrt{10}$ IN GEM L2 (Also used in GEM 5-9)

$$\sigma_{\text{GEM L2}}\ (\Delta g_s) = 4.63 \text{ mgals Commission Error}$$

GRAVITY ANOMALY DATA TEST CASES (Δg^*)	SATELLITE MODEL ERRORS EST $\sigma_{\text{Data}}\ (\Delta g_s)$	CALIBRATION FACTOR k
5° Equal Area Surf. Grav. (1976)	5.1 mgals	1.1
5° Equal Area Surf. Grav. (1981)	4.8	1.0
Δg ALTIMETER (OCEAN)		
1° x 1° SEASAT Altim. + S.G. Land (1981)	3.1	0.67
5° x 5° SEASAT Altim. + S.G. Land (1981)	3.0	0.65
5° x 5° SEASAT Altim. Only (1981)	3.0	0.65
5° x 5° GEOS-3 Altim. Only	3.2	0.69

*Data Sets Obtained from Rapp.

Table 5
Calibration of Satellite Model Error Estimates from Independent Solutions of
Sat Opical Data Only and Laser Data Only

CALIBRATION ($n \equiv$ degree ℓ)

$$RMS_n^2 = k_n^2 [\sigma_n^2 (OPT.) + \sigma_n^2 (LASER)]$$

RMS_n^2 = RMS of difference in coefficients of degree n between OPT. and laser solutions ($n \equiv \ell$)

k_n = Calibration factor

$$\sigma_n^2 = \sum_{m=0}^{n} [\sigma^2(C_{nm}) + \sigma^2 (S_{nm})] /2n+1)$$

Satellite Coefficient Errors

$$\sigma(C,S) = \sqrt{10}\ \sigma_{FORMAL}\ (C,S)$$

UNITS OF 10^{-9}

DEG n	RMS_n	σ_n(OPT)	σ_n(LASER)	k_n
3	14	18	11	.66
4	10	10	13	.62
5	17	21	23	.55
6	15	15	18	.66
7	24	25	24	.69
8	19	19	26	.59
9	24	25	30	.62
			AVERAGE	.63

Table 6
Gravity Model Comparison Using Independent Data from 24 Hour Satellites

	SAO				EUROPE		GSFC				
Weighted RMS Residual Accelerations	SE1	SE2	SE4	SE6	GRIM3	GRIM3B	GEM3	GEM7	GEM9	GEM10B	GEML2
	63.4	18.7	51.7	18.0	25.7	4.2	7.4	4.1	5.9	4.2	1.0

where the weighted residual acceleration is $(A_o - A_c/\sigma A_o)$

Contribution of Geopotential by Degree to Acceleration

ℓ	Contribution from Full Field	Contribution from Estimated Error of GEM-L2
2	3000×10^{-8}	2.6×10^{-8}
3	400	1.0
4	40	0.2
5	4	0.1
6	0.7	0.0

Table 7
Reliability of Lambeck/Coleman Error Estimate

DEGREE ℓ	RELIABILITY FACTOR $\frac{r_0}{\bar{\sigma}_\ell = 0}$	RELIABILITY FACTOR $\frac{r_2}{\bar{\sigma}_\ell = 2\sigma_\ell}$	PREDICTED SPREAD $\sigma_{e_\ell} = r_2\sigma_\ell$	LAMBECK/ COLEMAN ERROR ESTIMATE e_ℓ(GEM-L2)*	ERROR SPECTRUM σ_ℓGEM-L2)
2	40	60	±120	149 cm	2 cm
3	12	18	± 90	—197 cm	5 cm
4	8	12	± 72	— 91 cm	6 cm
5	6	9	±126	187 cm	14 cm
6	3.3	5	± 80	16 cm	
.					
.					
.					
10	1.3	2	± 70		35 cm

*Table 4 results from Lambeck/Coleman report, Reference Field SAO 1980.

Table 8
Gravity Model Comparison

LAGEOS LASER RANGE DATA
RMS OF FIT - THREE 7 DAY ARCS
(CM)

	2/1-9	2/9-16	2/22-30	TOTAL
GEM-L2	10 cm	12	8	10
GRIM3B	23	19	22	21
UNIV. OF TEXAS	25	22	20	22
GEM 9 *	21	19	20	20
SAO 77 *	113	105	128	114

* GRAVITY FIELD INDEPENDENT OF LAGEOS DATA.

GEODYN SYSTEMS DEVELOPMENT

Barbara H. Putney

OBJECTIVES

The purpose of the Geodyn Orbit Determination and Parameter Estimation, the SOLVE and ERODYN Programs is to recover geodetic and geophysical parameters from satellite and other data in a state-of-the-art manner.

BACKGROUND

In 1971 the NONAME and GEOSTAR programs were combined to create the GEODYN program. The SOLVE program was created at the same time. A few years later the ERODYN, error analysis program was written. The philosophy of the development of the software system has been maintenance of computer efficient, well-structured software, with appropriate orbit, earth and numerical models, using precise satellite measurement modeling and efficient numerical models, and performing careful benchmark procedures. This care has paid off in the production of several GEM's (Goddard Earth Models), precision station locations, improved tidal, GM, polar motion and earth rotation values, consistent baselines, and encouraging GRM simulations. Careful usage, analysis, and modeling using laser, altimeter and other satellite data from LAGEOS, SEASAT, STARLETTE, GEOS and BE-C satellites as well as many others has made these accomplishments possible.

RECENT ACCOMPLISHMENTS AND SIGNIFICANCE

Continued solutions for gravity field, pole positions, earth rotation, GM, and baselines have been made as part of the Crustal Dynamics Project. Some tidal parameters have been recovered as well. The eight digit station identification number has been incorporated in the software and new techniques for constraining monthly station parameters to each other is being developed. This is allowing the analysts even more flexibility in the shaping of solutions from monthly sets of normal equations and right-hand sides.

The GRM simulations have satisfied the analysts that with the simplistic model of the gravity field, GRM accurate gravity models can be obtained. It is expected that the Cyber 205 will enable finer detailed gravity models to be used.

Conversion of the Geodyn and Solve programs to the Cyber 205 computer has continued this year. The Geodyn II (vector rewrite) program had its first successful orbit generator run on December 13, 1983. Comparison running times are included in Figure 1. The initial timings are very encouraging. The next task is to process a data arc. The program is designed to run on both the IBM/Amdahl or the Cyber 205 computer, sharing a common source file and requiring a utility program to create the individual source programs.

This year the Solve program inversion routines have been fully vectorized and that portion of the program is running 25 times faster than the IBM 3081. It is truly remarkable that the Cyber 205 can fully invert the 1921 x 1921 matrix in 7 minutes or less. The details are in Figure 1. There is an I/O problem with this program and currently we are achieving only 33 percent CPU utlization. Two things can improve this situation, increased real memory (currently our Cyber only has one million words of memory) and concurrent I/O usage. We are working on the second item, but with only 2 channels on this system the best one can hope for is 50 percent CPU utilization. It is hoped that additional memory will be purchased for the machine. Work continues on vectorizing the data management areas of the program.

In addition to the Geodynamics/Crustal Dynamics Programs, the Geodyn software is being used by the AMPTE Project. In support of this effort this year, the Geodyn program has been sent to the Applied Physics Labortory in Laurel, Maryland; DFVLR in Germany; JPL in Pasadena, California. In support of Geodynamics/Crustal Dynamics research the program has been sent to Australia, The Netherlands, Japan, and Ohio State University.

FUTURE EMPHASIS

The Topex gravity field will require complete check out of existing models and the addition of others such as sea surface topography. This is going to be a large scale data processing effort and the software will be made as efficient as possible for this purpose.

The Geodyn II program needs to be completed and debugged for all currently implemented data types. New data types such as GPS should be implemented as well.

The Solve program needs to become a more flexible tool for Crustal Dynamics users. The handling of baselines, station solutions, polar motion and earth rotation solutions needs to be presented in a better way to make it easier for the analyst to easily distinguish between obviously poor and more promising solutions.

The Geodyn II program will be modified to have the year 2000 as the reference coordinate system and to achieve the other MERIT standards.

Every effort will be made, as resources allow, to continue to mold the software in a timely manner to support the needs of the scientific community determining earth models.

GEODYN TEST ORBIT GENERATOR RUN
2 DAY, 60 SEC STEP SIZE
36 × 36 GRAVITY MODEL, THIRD BODY EFFECTS,
STANDARD TIDES AND SOLAR RADIATION

	AMDAHL V-7	CYBER 205
GEODYN I	55 CPU SEC	
GEODYN IIS	1.8 CPU SEC	
GEODYN IIE	80 CPU SEC	
GEODYN IIE		5.4 CPU SEC
(ALL SMALL PAGES)		7.9 STU SEC

CYBER 7-10 TIMES FASTER THAN V-7

SOLVE TEST-FULL INVERSION

1921 PARAMETERS - 1 MATRIX INPUT

	IBM 3081	CYBER 205
SOLVE 8201.1 (9/82)	116.07 CPU MIN 31.45 I/O MIN	
SOLVE 8308.0 (9/83)		122.9 CPU SEC 356.1 STU SEC

CYBER 25+ TIMES FASTER THAN 3081

Figure 1. Time Comparisons of Vector/Scalar Geodyn and Solve Programs as of 2/84

D13

THE ERODYN AND QRPIG COMPUTER PROGRAMS

Theodore L. Felsentreger

OBJECTIVES

The role of the ERODYN computer program is to provide error analyses involving orbital, geodetic, and geophysical parameters. It has been designed to operate as a companion program to the GEODYN orbit determination and parameter estimation program. The Q R Partitioned Eigenvalue/Eigenvector analysis program (QRPIG) is designed to process symmetric matrices with an out-of-core partitioning algorithm for the eigenvectors and eigenvalues of the matrices.

BACKGROUND

The initial development of ERODYN was begun in the early 1970s, a few years after the GEODYN and SOLVE programs were created, and was intended to be a companion program to GEODYN. Basically, the purpose was to provide information on the effect of (assumed or actual) errors in certain parameters (unadjusted) upon the values of other parameters (adjusted) to be solved for. To accomplish this, ERODYN requires as input the matrix of normal equations ("E"-matrix) and, optionally, the matrix of variational partials ("V" matrix) as computed within GEODYN. In order to examine various partitionings of the total parameter set into adjusted and unadjusted parameters, the initial GEODYN run must have all parameters of interest "adjusted"; however, only one estimator iteration is required using "nominal" initial conditions to generate the required normal matrix and variational partials. These matrices are then subdivided within ERODYN into the appropriate adjusted and unadjusted partitions as specified by the ERODYN user.

As GEODYN's capabilities have been expanded and improved, an effort has been made to maintain the compatibility of ERODYN with GEODYN. In addition, many improvements have been made resulting in much more efficient use of computer resources. One of these improvements has been the application of a different algorithm for the eigenvalue/eigenvector option, resulting in more speed and reliability. A product of this change is a stand-alone eigenvalue/eigenvector program called QRPIG.

RECENT ACCOMPLISHMENTS AND SIGNIFICANCE

The GEODYN/ERODYN error analysis approach is extremely efficient in terms of computer resource utilization. A typical analysis problem would require multiple runs of an error analysis program using the same tracking schedule and problem geometry, but with different partitionings of the parameter set into adjusted and unadjusted parameters. However, with GEODYN/ERODYN the operations which are common to these multiple runs are performed only once by GEODYN and stored. ERODYN then does the matrix partitioning and linear algebra required for each individual error analysis run. In some instances, the "RSS iteration" feature of ERODYN can be used to achieve in a single run results which would usually require several.

The GEODYN/ERODYN error analysis approach also minimizes software design requirements. Any new measurement type or force model modification added to GEODYN is automatically included in the error analysis. This eliminates the requirement for separate coding, checkout and validation of both the error analysis and orbit determination programs.

The previous method for computing eigenvalues and eigenvectors within ERODYN employed the Jacobi algorithm and required that sufficient core storage be available to hold the entire matrix. The newly-implemented method uses an out-of-core partitioning algorithm, first reducing the (real, symmetric) matrix to a tridiagonal symmetric matrix using Householder transformations (Martin, et al, 1968), and then employing an iterative QR method to obtain the eigenvalues and eigenvectors (Bowdler, et al, 1968). This whole routine has been packaged as a stand-alone program (QRPIG).

FUTURE EMPHASIS

An effort is now underway to convert the ERODYN program to the Cyber 205 machine. The next step will be to optimize the program by making efficient use of the vector capabilities of the machine. It is anticipated that QRPIG will undergo the same conversion.

ERODYN can be an important tool for such missions as TOPEX and GRM, which will be quite sensitive to the gravity field of the Earth. Sensitivity analyses succh as those performed by ERODYN are extremely valuable in any research involving determination of Earth model parameters.

REFERENCES

Bowdler, H., R.S. Martin, C. Reinsch, and J.H. Wilkinson, "The OR and QL Algorithms for Symmetric Matrices", Num. Math. 11, pp. 293-306, 1968.

Martin, R. S., C. Reinsch, and J. H. Wilkinson, "Householder's Tridiagonalization of a Symmetric Matrix", Num. Math. 11, pp. 181-195, 1968.